Imperial College London

Causal Set Theory and the Benincasa-Dowker Conjecture

Ansh Bhatnagar

Supervisor: Fay Dowker

Abstract

Causal Set Theory (CST) is an approach to quantum gravity which asserts that spacetime is fundamentally a locally finite partially ordered set that encodes a causal ordering between elements. We review the causal sets programme and key developments such as the Benincasa-Dowker-Glaser (BDG) causal set action S_{BDG}. We then turn our attention to the Benincasa-Dowker conjecture: a conjecture which claims that, in the continuum limit, the mean of the random discrete action (i.e. the BDG action calculated on a causal set $\mathcal{C}$ generated by sprinkling a globally hyperbolic Lorentzian manifold $\mathcal{M}$) gives the usual bulk Einstein-Hilbert action term calculated on $\mathcal{M}$ plus a boundary term that is the volume of the intersection between the past and future boundaries of $\mathcal{M}$. We provide new evidence for this conjecture with calculations on the 2D flat and curved trapezium spacetimes, 2D overlapping causal diamonds spacetime, and the 4D flat cone spacetime. We also show indications that the conjecture holds for the 4D curved cone spacetime.

Submitted in partial fulfilment of the requirements for the degree of Master of Science of Imperial College London

Theoretical Physics Group
Department of Physics
September 2021

Contents

Chapter 1

Introduction

1.1 Quantum Gravity

Arguably the most central problem facing fundamental physics today is the quest for a theory of quantum gravity. Currently, fundamental physics rests on two pillars that have achieved great success in their realms of applicability: general relativity (GR) and quantum field theory (QFT). While the former has played a crucial part in our understanding of the universe, acting as a bedrock theory for the ΛCDM model of cosmology, it essentially predicts its own downfall by throwing up singularities when probed at the smallest scales; at the centres of black holes and at the Big Bang. Similarly, while QFT facilitates the Standard Model (SM) of particle physics and has delivered the most precise experimentally verified predictions in all of physics, it fails to provide a functioning theory of gravity.

The issues with merging these theories arise most apparently from their conflicting fundamental nature. GR is a classical, deterministic theory which models the universe as a 4D Lorentzian manifold: a construction that is continuous and not discrete. This manifold is allowed to curve in the presence of matter-energy according to the Einstein Field Equations (EFE). The curvature of the manifold then dictates the dynamics of matter-energy via the geodesic equation. QFT, meanwhile, requires the bosonic and fermionic fields of the SM to lie on a flat, special relativistic Minkowski "stage", making it inherently difficult to then quantise that stage itself. The quantum nature of QFT is also incompatible with GR, which can be used to make deterministic predictions at the smallest scales as long as singularities are avoided.

A further issue comes from the impracticality of experimental guidance; with previous theoretical developments, we have often had experiment to guide us. However the fundamental scale of quantum gravity is presumed to be the Planck scale: for example, in units where $c = 1$, the Planck length is $l_p \sim \sqrt{G\hbar} \sim 10^{-35}$m which is 20 orders of magnitude smaller than the length scale of a proton. The Planck energy meanwhile is $E_p \sim 10^{19}$ GeV, whereas the LHC can access energies of only 10^4 GeV [1], which is 15 orders of magnitude away from experimentally probing quantum gravity. In fact if we wanted to build a detector to detect the conjectured quantum of gravity, the graviton, according to one estimate it may have to be as massive as Jupiter [2] making it anything but a feasible experiment in the foreseeable future.

For now, quantum gravity research remains highly theoretical, without experiment to guide it, and thus encompasses a multitude of vastly varying approaches.

1.2 The problems with the continuum

There are many reasons to suggest why a continuous manifold, as in GR, is not fundamental. For example, continuity implies that the physics extends to arbitrarily small scales, when we already know that ideas of length become meaningless below the Planck scale.

In QFT, a continuum implies that there are ultraviolet modes for the quantum field that remain unbounded by any energy scale, which creates divergences that may be dealt with by renormalising the theory using a finite number of counter-terms in the Lagrangian to absorb those divergences. However, when we attempt to canonically quantise the graviton field, we encounter an issue: the divergences due to the ultraviolet modes cannot be absorbed away by a finite number of counter-terms, making the theory non-renormalisable. If spacetime had a lower limit for distance scales, there would be a physical energy cut-off which would allow for the taming of any divergences.

In GR, the issue of arbitrary small scales appears near the black hole singularity. In this immediate neighbourhood where the curvature is incredibly high, GR continues to provide predictions which we already know can't be correct as GR is not a quantum theory. For similar reasons, GR should also fail in the very early universe.

These are just some of the arguments against our current conceptualisation of a continuum spacetime, motivating the idea of a fundamentally discrete spacetime as a starting point for a theory of quantum gravity.

Chapter 2

Causal Set Theory

For this chapter, we turn our attention to the focus of this dissertation: the causal set approach to quantum gravity. This programme was first formally proposed by Bombelli, Lee, Meyer and Sorkin in their seminal 1987 paper [3], which in turn was heavily influenced by earlier developments from Myrheim [4], Hawking [5], and Malament [6] to name a few.

2.1 Spacetime as a causal set

The key assertion of Causal Set Theory (CST) is that the familiar (3+1)-dimensional Lorentzian manifold $\mathcal{M}$ of GR is nothing more than an emergent phenomenon of the more fundamental causal set $\mathcal{C}$: a set of discrete elements partially related to one another by their causal relationships. In a sense, the manifold becomes discrete, and the elements can be considered to be 'atoms' (in the etymological meaning of the word, derived from the Greek 'atomon' meaning indivisible) of spacetime. These abstract elements are analogous to the spacetime points from the manifold, with the main distinction being that, at the causal set level, they cannot be labelled by a coordinate system. This is due to the fact that the very notion of coordinates is intrinsically tied to that of smooth manifolds; the points on the manifold are only given coordinates in reference to a certain chart.

2.1.1 Motivation for a discrete spacetime

The 'discrete manifold' is not an entirely novel idea; in fact, it was discussed by Riemann [7] in 1873

> "Now it seems that the empirical notions on which the metrical determinations of space are founded, the notion of a solid body and of a ray of light, cease to be valid for the infinitely small. We are therefore quite at liberty to suppose that the metric relations of space in the infinitely small do not conform to the hypotheses of geometry; and we ought in fact to suppose it, if we can thereby obtain a simpler explanation of phenomena. The question of the validity of the hypotheses of geometry in the infinitely small is bound up with the question of the ground of the metric relations of space. In this last question, which we may still regard as belonging to the doctrine of space, is found the application of the remark made above; that in a discrete manifoldness, the ground of its metric relations is given in the notion of it, while in a continuous manifoldness, this ground must come from outside. Either therefore the reality which underlies space must form a discrete manifoldness, or we must seek the ground of its metric relations outside it, in binding forces which act upon it."

and Einstein [8] in 1916

> "But you have correctly grasped the drawback that the continuum brings. If the molecular view of matter is the correct (appropriate) one, i.e., if a part of the universe is to be represented by a finite number of moving points, then the continuum of the present theory contains too great a manifold of possibilities. I also believe that this too great is responsible for the fact that our present means of description miscarry with the quantum theory. The problem seems to me how one can formulate statements about a discontinuum without calling upon a continuum (space-time) as an aid; the latter should be banned from the theory as a supplementary construction not justified by the essence of the problem, which corresponds to nothing "real". But we still lack the mathematical structure unfortunately. How much have I already plagued myself in this way!"

both of whom were integral to our current understanding of the universe as a smooth manifold. These concerns around the continuum were well-motivated; for Riemann, he saw no reason for why the continuum of physical space should extend all the way down to scales of the extremely small, in the same way that solid objects are made up of indivisible elements. In fact, he posits that the discrete manifold picture possesses an advantage in that

the metric is intrinsic to the manifold, and not a separate object like it is for the continuous manifold. This idea, applied to causal sets, is explored later in this section.

Meanwhile, Einstein made his remarks during the early years of quantum mechanics, when it had become evident that discreteness and probability played an important role in the universe, making his newly formulated theory of GR incompatible with the quantum picture. As discussed in the Introduction, this incompatibility would further be exacerbated by the infinities arising in QFT. These reasons alone form a strong incentive to investigate the discretisation of spacetime.

2.1.2 Definition of a causal set

A more formal definition of causal sets makes use of the axioms as specified by Bombelli et al. [3][9] and the notation employed by Benincasa and Dowker [10].

Definition 1. A causal set $\mathcal{C}$ (often referred to as 'causet' for short) is a partially ordered set ('poset' for short) with a binary order relation $\preceq$, which is

1. *Transitive:* If $x \preceq y$ and $y \preceq z$ then $x \preceq z$, $\forall x, y, z \in \mathcal{C}$
2. *Acyclic:* If $x \preceq y$ and $y \preceq x$ then $x = y$, $\forall x, y \in \mathcal{C}$
3. *Locally finite:* $|I(x, y)| < \infty$, $\forall x, y \in \mathcal{C}$

where $I(x, y)$ is the order interval between causet elements x, y, defined as $I(x, y) = \{z | x \preceq z \preceq y\}$ and analogous to the Alexandrov causal interval $A(x, y)$ for $x, y \in \mathcal{M}$ (see Appendix A). Also, the function $n(x, y) = |I(x, y)| - 2$ will prove useful in Chapter 3. We will write $x \prec y$ if $x \preceq y$ and $x \neq y$.

2.1.3 Causal structure and the CST slogan

The foremost question when first investigating CST is: does a causal set retain all the physically relevant information that the emergent manifold gives us? After all, if we lose information when moving from what is meant to be an emergent phenomenon to what is supposed to be a more fundamental structure, that structure cannot be more fundamental and there would be no further reason for us to investigate the theory. New theories need to retain all the physical results of older theories, but also provide us with new insight in areas where the old theories failed.

There is good reason for us to suspect that causal sets retain the same information as the manifold - but only at scales larger than the discreteness scale of the causet. For scales on the order of the discreteness scale or smaller, causets necessarily lose the information of the manifold; however this is not expected to be physically relevant information. This insight first came by considering the continuous manifold as a poset of all the spacetime points, also referred to as an event-set M, alongside the causal relation $\prec$. This means the manifold $\mathcal{M}$ is replaced by $(M, \prec)$, which is similar to a causal set apart from M being the set of points on $\mathcal{M}$ and thus being uncountably infinite. In order to distinguish between this set of events and the discrete causal set, we refer to the former as the continuum causal poset.

A result by Zeeman [11] showed that, if we take a *chronological* poset $(M, \prec\!\prec)$ where $x \prec\!\prec y$ denotes a chronological relation between x and y, i.e. that a timelike curve exists between x and y, we can define a chronological automorphism f to be one that preserves the chronological poset structure,

$$f : M \to M,\ x \prec\!\prec y \to f(x) \prec\!\prec f(y),\ \forall x, y \in M \tag{2.1}$$

This group of chronological automorphisms $G_{\prec\!\prec}$ was then shown to be isomorphic to the group of inhomogeneous Lorentz transforms and dilatations G_{Lor} on M for $d > 2$. Note that, while Zeeman refers to f as a causal automorphism, we make a distinction between chronological and causal, however in the same paper Zeeman shows that the result holds whether or not the group of chronological automorphisms $G_{\prec\!\prec}$ is considered or the more general group of causal automorphisms $G_{\prec}$ is considered. This crucial result showed that the Lorentz group arises naturally from the idea of causality, and implies that causal relations may be enough to recover the Lorentzian manifold.

HKMM Theorem

This was further generalised by Hawking, King, McCarthy [5] and Malament [6] (HKMM), with Surya referring to these collective results as the HKMM theorem [9]:

"If a chronological bijection f exists between two d-dimensional spacetimes which are both future and past distinguishing (FPD), then these spacetimes are conformally isometric when $d > 2$."

which, due to a result by Levichev [12], was shown to be equivalent to the statement

where 'chronology' is replaced with 'causality'. In this case, FPD spacetimes are a very general class of spacetimes $\mathcal{M}$ where, if points $p, q \in \mathcal{M}$ share the same chronological past and future $I^{\pm}(p) = I^{\pm}(q)$, then that implies $p = q$.

The HKMM theorem illustrates that if the causal structure of two spacetimes is identical, then they must be conformally isometric. As the metric is the basis of the Einstein Field Equations and GR, the two spacetimes are (almost!) physically the same. The continuum causal poset $(M, \prec)$ therefore carries the same information as the metric up to a conformal factor which encodes the volume of the space.

There is a problem here: causal structure alone, in this continuum case, isn't enough to return the same information as can be found in the metric. Fortunately, a *discrete* causal poset provides the answer; if we take the amount of elements to be locally finite, as in Axiom 3 of the definition of a causal set, we can simply *count* the number of elements in order to find the volume. This is impossible with the continuum causal poset, as it is uncountably infinite. We see that the discretisation of the manifold follows naturally from the HKMM theorem, if one intends to form a theory where causality is the fundamental essence of spacetime.

This elegant formulation has been the main driver of CST; so central is it to its foundation that Sorkin coined the 'CST slogan':

"Order + Number = Geometry"

2.2 Hasse diagrams

Causal sets are often depicted pictorially as Hasse diagrams, a type of diagram used for visualising partially ordered sets more generally. The causet elements may be depicted abstractly (Fig. 2.1), or they may be depicted as points on a spacetime manifold (such as in Fig. 2.2). While causet elements themselves have no coordinates in the theory, elements of 'manifold-like' causets can be faithfully embedded onto a manifold.

Definition 2. A faithful embedding f of a causal set $\mathcal{C}$ is one that maps the elements onto a Lorentzian manifold $\mathcal{M}$ while preserving the causal structure (i.e. if for $x, y \in \mathcal{C}$, $x \prec y$, then for $f(x), f(y) \in \mathcal{M}$ there exists a future directed causal curve between $f(x)$ and $f(y)$, and likewise if there is no relation between x and y, $f(x)$ and $f(y)$ are spacelike separated) and at a density where, on average, the number of causet elements in a region is equal to the volume of that region in fundamental units.

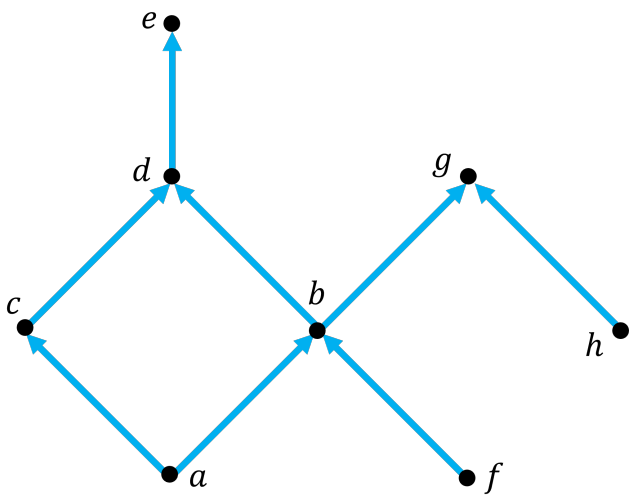

Figure 2.1: A Hasse diagram depicting a simple 8 element causal set. Arrows indicate the partial ordering of the causal relations; e.g. $a \prec c$. Only links are depicted; e.g. $a \prec b$ is a link, however $a \prec e$ is inferred from the axiom of transitivity. We also see that there exist elements with no causal relations between them, e.g. $f \not\prec h$ and $h \not\prec f$.

Hasse diagrams such as in Fig. 2.1 ignore causal relations that are not *links*. We say that, for $x, y \in \mathcal{C}$, $x \prec y$ is a link if there exists no element $z \in \mathcal{C}$ such that $x \prec z \prec y$. It is in a sense the 'fundamental' causal relation - and all other causal relations can be inferred by transitivity.

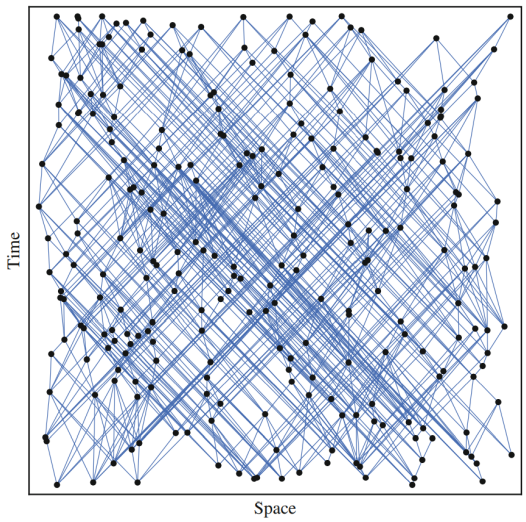

Figure 2.2: A Hasse diagram from Dowker [13] depicting causal set elements 'sprinkled' as points on a manifold (in this case, flat 2D Minkowski space).

2.2.1 The 'size' of a causet element

While the elements of a causal set don't have a size per se, and the links don't have lengths, the average density ρ at which elements are embedded in the emergent manifold would be reciprocal to a fundamental Planck scale volume V_p. Thus it follows that any given volume V_p in the spacetime is expected to contain one causet element, and this in a way can be thought of as an average 'size' of the element.

Naturally, in units where $c = 1$, we expect that $V_p \sim (l_p)^d$, and thus the spacetime 'length' of a link is on the order of the Planck length.

2.3 Emergence of the spacetime manifold

At the centre of CST is the assumption that the continuum spacetime arises as an emergent phenomenon from the fundamental causet spacetime. But how do we formalise this statement? Given a causet, how do we figure out what sort of manifold it corresponds to?

An initial stumbling block is that the definition of a causet is incredibly general; there is no requirement for a causet to be 'manifold-like'. The set of all causets therefore contains an enormous amount of causets that we may struggle to embed into a continuum Lorentzian manifold. We therefore restrict our discussion to the set of all 'manifold-like' causets.

Definition 3. A manifold-like causet $\mathcal{C}$ is one that may have been produced by a sprinkling of a Lorentzian manifold $\mathcal{M}$.

A sprinkling is a method that produces a causet $\mathcal{C}_\mathcal{M}$ from a given manifold $\mathcal{M}$, by choosing a countable (finite or infinite) number of points on $\mathcal{M}$ which become the elements of the causal set. The causality relations are then taken from the causal order on the manifold, which combines with the elements to create a causet $C_\mathcal{M}$. The underlying $\mathcal{M}$ can then be discarded as it is no longer required.

Then, for a specific manifold-like causet $\mathcal{C}$, we say that it is well-approximated by a given manifold $\mathcal{M}$ if it might have been produced by a sprinkling on $\mathcal{M}$. This means that, at volume scales $V \gg V_p$, the geometry of manifold $\mathcal{M}$ is indeed an emergent phenomenon of the fundamental causet $\mathcal{C}$.

2.3.1 Sprinklings

How sprinklings are carried out is an important question. Which spacetime points get to become part of the newly generated causet, and why? One of the most primitive methods that one may think of sprinkling is by placing the points in the form of a regular grid. In this way, they appear to be evenly spaced - but only in a specific reference frame. Under a Lorentz boost, the regularly spaced grid of points will be distorted such that the uniformity of density disappears and the grid is no longer evenly spaced. It is clear that this lattice spacing is not Lorentz invariant.

However, if we instead sprinkled points using the Poisson distribution with average density ρ (i.e. the expected number of causet elements in a spacetime volume V is $\langle n \rangle = \rho V$), this would be 'Lorentz invariant'. This Lorentz invariance is in the sense that, while the actual points have a change of coordinates, both the pre-Lorentz boost and Lorentz boosted distribution of points would follow the Poisson distribution

$$P_\rho(n, V) = \frac{(\rho V)^n}{n!} e^{-\rho V} \tag{2.2}$$

where $P_\rho(n, V)$ is the probability at sprinkling density ρ of finding n elements in a volume V.

The randomness of the Poisson distribution invites the idea of an equivalence class of causets. If two causets $\mathcal{C}$ and $\mathcal{C}'$ can both be considered to be well approximated by the same Lorentzian manifold $\mathcal{M}$, then we can write $\mathcal{C} \sim \mathcal{C}'$ and they can both be considered to be members of the equivalence class $[\mathcal{C}]$, where $\mathcal{C}$ is the representative. The two causets then have physical differences at the Planckian scale, but at larger scales they present essentially the same emergent spacetime continuum. In an apt analogy by Surya [9], the elements of the equivalence class $[\mathcal{C}]$ can be thought of as 'microstates' of the macrostate corresponding to the emergent manifold $\mathcal{M}$.

2.3.2 The 'hauptvermutung' of CST

The relationship where multiple causets can be well approximated by the same manifold naturally begs the question: can two or more different manifolds well approximate a single causet? We have been operating under the implication that, given a causet spacetime, there exists a unique physical emergent spacetime continuum. If this were not true, the key assertion of CST that the continuum is nothing more than an emergent phenomenon would

collapse.

The key words there, however, are 'physical' and 'emergent'. We can imagine that two manifolds that differ only at non-physical scales (i.e. the Planck scale, where GR ceases to be a valid physical description) could generate the same causal set. This leads neatly into what is called the 'hauptvermutung', or 'fundamental conjecture' of CST. It states that:

"A causet $\mathcal{C}$ can be well approximated by two distinct Lorentzian manifolds $\mathcal{M}$ and $\mathcal{M}'$, if and only if $\mathcal{M}$ and $\mathcal{M}'$ are approximately isometric."

'Approximate isometry' here implies that the spacetimes are identical at volume scales $V \gg V_p$. They may differ only at the Planckian scale, in which case it is easy to understand how those distinct spacetime continua could end up plausibly generating the exact same $\mathcal{C}$ via sprinkling.

There are a number of statements that have been made that rest on something that is yet to be rigorously defined. What does it mean for a continuum to 'plausibly' generate a causal set? The rigorous formalisation of this statement and the idea of 'well approximated' is something that is ongoing, but in the meantime it provides motivation for the sort of behaviour we require CST to have.

2.3.3 Coarse graining

It may be the case that a finalised version CST would allow for causal sets that don't directly satisfy the condition of being well approximated by the continuum manifold; in that case, we introduce an intermediate stage in order to link the causet with the emergent continuum. This intermediate stage would be another causet $\mathcal{C}_p$ that is not the underlying fundamental causet $\mathcal{C}$; rather, it is a 'coarse-graining' of $\mathcal{C}$.

This coarse-graining would be achieved by selecting at random a subset of the original causet elements, and retaining the relevant causal relations. Thus $\mathcal{C}_p \subset \mathcal{C}$ and it would be characterised by a 'survival probability' $p = |\mathcal{C}_p|/|\mathcal{C}|$. We can again think of the equivalence class of all the causets that can be produced by coarse graining the fundamental causet with a survival probability p, labelling it $[\mathcal{C}_p]$. The equivalence class $[\mathcal{C}_p]$ may then be the object that forms the link between the fundamental causet and the emergent continuum; if instead the members of $[\mathcal{C}_p]$ can plausibly be produced by sprinkling $\mathcal{M}$ at a lower density $\rho_p = p\rho$, then we could say that $\mathcal{M}$ emerges from the fundamental causet $\mathcal{C}$.

This looser condition may admit more causets into the physical theory than would oth-

erwise be allowed; these additional causets would not be manifold-like at the Planck scale.

2.3.4 Dimension estimators

Dimensionality is not an innate feature of a causet. Rather, it is a feature coupled with the emergent continuum. However, if the hauptvermutung holds true, this continuum is macroscopically unique and thus the dimensionality of the emergent continuum can be associated with the underlying causet itself.

There are numerous dimension estimators that have come through in the literature. One of the earliest formulated is called the Myrheim-Meyer estimator [4][14], with Myrheim's work on this preceding the formalisation of CST by Bombelli et al. by almost a decade.

Myrheim-Meyer dimension

The Myrheim-Meyer estimator works as follows; take an order interval $I(x, y)$ between causet elements $x, y \in \mathcal{C}$ for which $x \prec y$. Then $N = |I(x, y)|$ is the number of elements in the order interval, and R is taken to be the number of pairs $a, b \in I(x, y)$ for which $a \prec b$. Then the dimension estimator is calculated using the analytic continuation of the binomial coefficient $\binom{n}{k}$ to real numbers, such that [15]

$$\frac{R}{\binom{N}{2}} = \frac{3}{2}\binom{\frac{3d}{2}}{d}^{-1} \tag{2.3}$$

which can be rearranged as

$$\frac{R}{N(N-1)} = \frac{\Gamma(d+1)\Gamma\left(\frac{d}{2}\right)}{4\Gamma\left(\frac{3d}{2}\right)} \equiv f(d) \tag{2.4}$$

This equation can then be inverted such that

$$d = f^{-1}\left(\frac{R}{N(N-1)}\right) \tag{2.5}$$

provides a good estimate of the dimension of the causet as long as $N \gg (27/16)^d$. This is a powerful result; it is possible to estimate the dimensionality of a causet by simply counting the number of elements in an order interval, and the number of causal relations.

Midpoint-scaling dimension

Another dimension estimator is called the midpoint-scaling estimator, based around finding the midpoint of the order interval $I(x, y) \subset \mathcal{C}$ [14][16]. This midpoint z is such that, for $x \prec z \prec y$, we can construct new order intervals $I_1(x, z)$ and $I_2(z, y)$ such that $N_1 = |I_1(x, z)|$ and $N_2 = |I_2(z, y)|$.

We then choose N_{mid} to be the smaller of N_1 and N_2. Now, the causet element z is chosen such that it maximises N_{mid} and thus z is expected to be the midpoint of the order interval $I(x, y)$. The dimension of $\mathcal{C}$ is then

$$d \approx \ln\left(\frac{N}{N_{\text{mid}}}\right) \tag{2.6}$$

Checks for physically relevant causets

These two estimators have been found to be invariant under coarse graining, which is evidently a desired property for an ideal dimension estimator. Reid tested these estimators for numerous conformally flat spacetimes [16], and outlined a method that utilises these estimators to check if a given causal set $\mathcal{C}$ can be faithfully embedded into 'physically relevant' spacetimes.

This method goes as follows:

1. Create a large order interval $I(x, y) \in \mathcal{C}$.

2. Calculate the average dimension $\langle \mathbf{d} \rangle$ by computing the dimension of several small $(3 < N < 100)$ sub-intervals of $I(x, y)$ using either the Myrheim-Meyer estimator or the midpoint scaling estimator, and averaging over them.

3. Repeat Step 2 for causets created by sprinkling Minkowski spacetimes of different dimensions.

4. Compare the average dimension $\langle \mathbf{d} \rangle$ to the average dimensions of the sprinkled Minkowski spacetimes as a check for the causet being locally Minkowski.

As we expect physically relevant spacetimes to be locally flat, this method should be a check for whether or not given causets can give rise to emergent physically relevant spacetimes.

2.4 The space of causets

In Section 2.3, we briefly mentioned that the set of all causets contains an enormous number of non-manifold-like causets. This space, known as Ω, has only a small subspace $\Omega_{\mathcal{M}}$ that consists of manifold-like causets. The rest of Ω is dominated by the Kleitman-Rothschild (KR) causets [17].

2.4.1 Kleitman-Rothschild causets

These causets consist of three 'layers', such that for a causet of cardinality n, there are approximately $n/4$ elements in the 'bottom' and 'top' layers, and $n/2$ elements in the 'middle' layer. The links exist only between the bottom and middle layers or middle and top layers, but never between the bottom and top layers (as otherwise that element in the top layer would be classified in the middle layer).

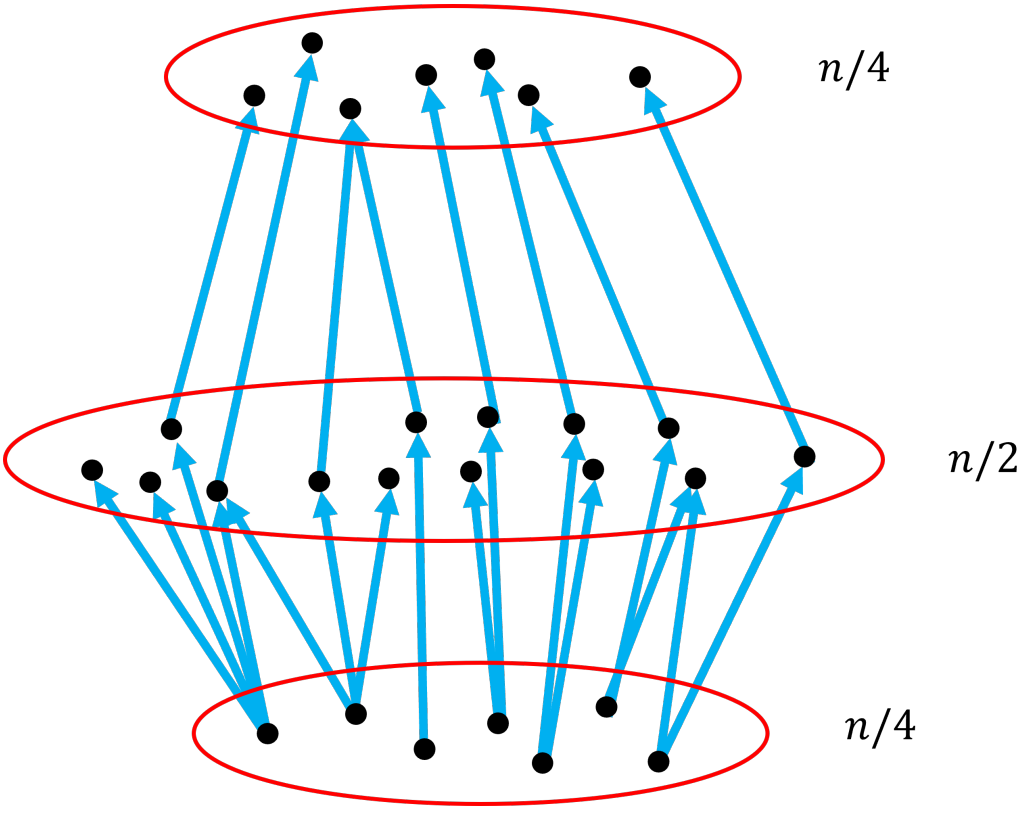

Figure 2.3: A Hasse diagram of a KR causet of cardinality $n = 28$, with $n/4$ elements in the 'bottom' and 'top' layers, and $n/2$ elements in the 'middle' layer.

We denote the space of causets of cardinality n as Ω_n. As $n \to \infty$, the proportion of this space that consists of KR causets tends to one, meaning that KR causets are by far the

'typical' causet.

There also exist other layered causets that are non-manifold-like, forming a dominance hierarchy with KR causets at the top [9]. These other classes include the bilayered causets, where the only causal relations are links and the causet can thus be split into a past layer and a future layer.

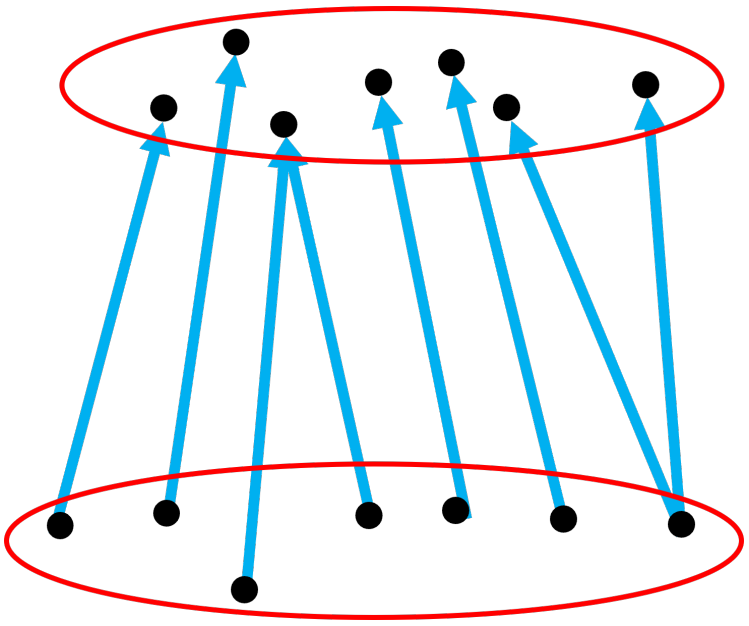

Figure 2.4: A Hasse diagram of a bilayer causet with the past and future layers indicated.

These causets are undesirable for the theory as they are not manifold-like, yet we know that our current spacetime is indeed manifold-like. Despite this they dominate the space of causets. An important question that CST must answer is then: why do these non-manifold-like causets not arise in the macro scale theory? And why does the underlying causet of our universe approximate as a 4D manifold? These questions could be answered by outlining a dynamics for causal sets that favours manifold-like causal sets, particularly at larger scales, and tends to GR dynamics in the macroscopic scale.

2.5 Dynamics

So far we have defined causets and studied how the spacetime continuum may emerge from an underlying fundamental causet. However, we are still missing the dynamics of the theory, which is key if we are to form a complete theory of quantum gravity. Just as GR defined the dynamics of the spacetime continuum through the Einstein Field Equations, so too

must we define the dynamics of causal set. A number of models for the dynamics have been developed, particularly in the last couple decades. These are called 'sequential growth' models and they dictate how a causal set can grow by adding new elements and causal relations.

These are split into two classes; Classical Sequential Growth (CSG) and Quantum Sequential Growth (QSG).

2.5.1 Classical Sequential Growth

CSG was pioneered by Rideout and Sorkin [18], based on a classical, stochastic process for growing causal sets. Elements are added to an initial causal set, one at a time in sequence, with its causal relations to existing elements being decided probabilistically. If a causet $\mathcal{C}_{n+1}$ of cardinality $n+1$ has been generated by adding an element to a causet $\mathcal{C}_n$, we say that $\mathcal{C}_{n+1}$ is a 'child' of the 'parent' causet $\mathcal{C}_n$.

The poscau

This structure gives rise to a partial order on the set of causets, with the poset of causets being referred to as the 'poscau'. A poscau $\mathcal{P}$ is depicted as a Hasse diagram of Hasse diagrams in Fig. 2.5.

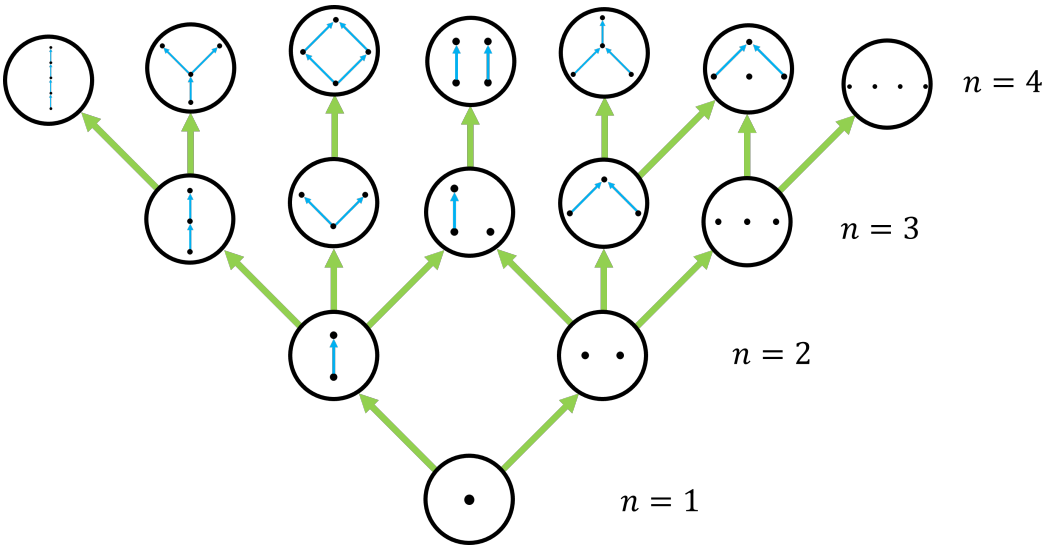

Figure 2.5: A Hasse diagram of a poscau $\mathcal{P}$, showing the partial order on causets generated by CSG. n indicates the cardinality of the causets at each row. While all possible causets are shown for $n \leq 3$ (apart from the empty causet), only a selection of the possible $n = 4$ causets are shown in the diagram.

While the addition of elements can 'begin' at any size causet, it is natural to start with the empty set $\emptyset$ or the one element causet, as in Fig. 2.5. This can be thought of as depicting the possible routes that a universe could take after the Big Bang.

Transitive percolation

The set of all causets of cardinality n is labelled as Ω_n, and the transition from Ω_n to Ω_{n+1} is referred to as a 'stage', i.e. causet elements are added in stages. At each stage, the transitive percolation method as defined by Rideout and Sorkin goes as follows. For a causet $\mathcal{C}_n$,

1. Add a new element y to the set.
2. For each pre-existing element x_i for integer $i \in [1, n]$, the probability that y is the causal successor of x_i is p.
3. The rest of the causal relations follow from the property of transitivity. We have now formed a new causet $\mathcal{C}_{n+1}$.

We see that n ends up acting as a label for some sense of external 'time' parameter that passes as the causet grows. In transitive percolation, there is nothing to say that p must remain constant throughout the various stages; p could change as a function of n.

CSG as a Markov process

We can also consider CSG to be a Markov process where each element $\mathcal{C} \in \mathcal{P}$ is a 'state', and the link between two causets is assigned a transition probability p. This Markov process is such that the only transitions that exist from a causet $\mathcal{C} \in \Omega_n$ are to those in Ω_{n+1}, and this is further restricted to only the causets of Ω_{n+1} that are children of $\mathcal{C}$. In this view, the microscopic mechanism of assigning probability to a certain causet transition (such as in the outlined method for transitive percolation) can be neglected in favour of any generic map between the set of poscau links to a real number in $[0, 1]$.

As the underlying principles of CSG have been laid out, we will now turn our attention to the physical considerations.

Condition of internal temporality

This condition simply states that the growth process cannot add a new element to the past of any existing elements, i.e. at stage n, the newborn element $x \not\prec y, \forall y \in \mathcal{C}_n$. This condition

doesn't just allow for new elements to be causal descendents of existing elements: they can also be causally unrelated to existing elements, and in fact they can be causally unrelated to *all* pre-existing elements, as seen in the descendent causets on the right hand side of Fig. 2.5.

Labelling

As causet elements aren't labelled, the exact order that the elements are added to get to a certain $\mathcal{C} \in \mathcal{P}$ should not be of any physical significance. However, in order to handle the causets mathematically, we can imagine a map $l : \mathcal{C} \to \mathbb{N}$ such that each causet element is assigned a label associated with the order they were added to the causet. For example, if an element x is added at stage n, then $l(x) = n$. The element in the single-element causet is therefore given the label 0, as the second element in the causet is the one that is added at stage 1.

The partial ordering can then be carried over to $l(\mathcal{C})$, such that it is referred to as a 'naturally labelled causet'. As this labelling shouldn't be physically relevant, we think of naturally labelled causets that differ only by a permutation of the labellings to be equivalent to the same causet; it is the causal structure that matters, not the labelling.

Condition of general covariance

The formalisation of the idea that a labelling shouldn't be physically relevant is the condition of general covariance. Treating CSG as a Markov process, the growth of a causet should be path independent. What we mean by this is that the probability of transitioning from the empty state $\emptyset$ to a causet $\mathcal{C}$ should be the same regardless of what intermediate states are taken to get there. Therefore the probabilities assigned to the transition links are such that their product along a path should equate to the product of the transition probabilities along a different path with the same start and end state.

Bell causality

This restriction is a formalisation of the idea that the birth of a new element should only be affected by the elements to its past. At the dynamical level, this means that the probability of any given transition $p(\mathcal{C}_n \to \mathcal{C}_{n+1})$, where a newborn element x is added, should not be affected by the spectator set $\text{spec}_n(x) = \{y \in \mathcal{C}_{n+1} | y \not\preceq x\}$: the set of pre-existing

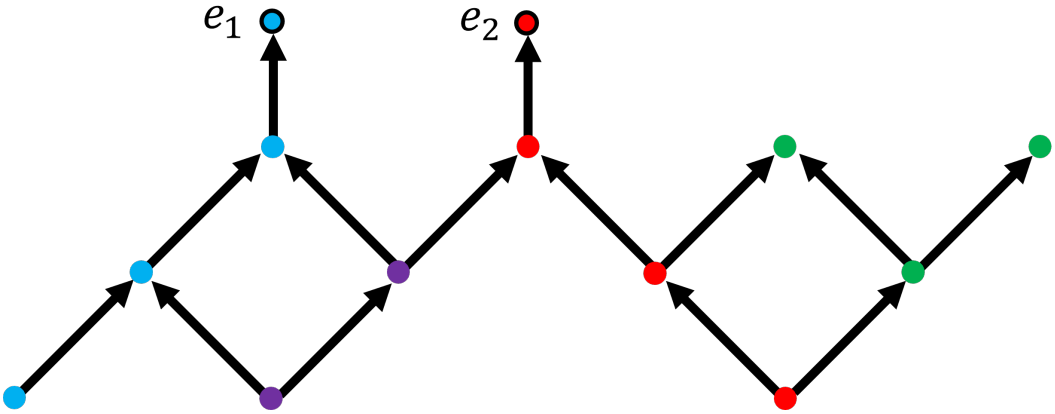

Figure 2.6: A Hasse diagram of an example causet $\mathcal{C}$, with newborn elements e_1 and e_2 being shown as the blue and red bordered circles respectively. The elements that comprise $\text{prec}(e_1)$ are shown as non-bordered blue and purple circles, and the elements that comprise $\text{prec}(e_2)$ are shown as non-bordered red and purple circles, with the purple circles comprising the intersection of the two precursor sets. The elements of the spectator set of both transitions $\text{spec}(e_1, e_2)$ are shown as green circles. These are the elements that do not form part of $\mathcal{C}' = \text{prec}(e_1) \cup \text{prec}(e_2)$.

elements causally unrelated to the newborn element. Similarly, we define the precursor set $\text{prec}_n(x) = \{y \in \mathcal{C}_{n+1} | y \prec x\}$ as the set of elements in the past of the newborn element.

Now consider the ratio of the probabilities of transition between the same causet $\mathcal{C} \in \Omega_n$ to new causets $\mathcal{C}_1, \mathcal{C}_2 \in \Omega_{n+1}$. This ratio should be equivalent to the ratio with the same elements being born without the spectator set; if it wasn't, then the presence of the spectator set would be affecting the likelihood of new elements being birthed even though they are causally unrelated to them.

To formalise this Bell causality condition, we define $\mathcal{C}' = \text{prec}_n(e_1) \cup \text{prec}_n(e_2)$ as the union of the precursor sets of the two elements e_1 and e_2 birthed in the transitions $\mathcal{C} \to \mathcal{C}_1$ and $\mathcal{C} \to \mathcal{C}_2$ respectively. Then $\mathcal{C}'_1$ is $\mathcal{C}'$ with e_1 added just as in the former transition, i.e. e_1 gets linked to the analogous elements in $\mathcal{C}'$, and similarly for $\mathcal{C}'_2$. Then the Bell causality condition is

$$\frac{p(\mathcal{C} \to \mathcal{C}_1)}{p(\mathcal{C} \to \mathcal{C}_2)} = \frac{p(\mathcal{C}' \to \mathcal{C}'_1)}{p(\mathcal{C}' \to \mathcal{C}'_2)} \tag{2.7}$$

These conditions ensure that CSG can be viewed as a physically meaningful process, however we already know that CSG isn't going to be the 'final answer'; it is merely a useful stepping stone on the way to quantum dynamics, and a full development of the causal sets programme as a theory of quantum gravity.

2.5.2 Quantum Sequential Growth

CSG can be extended into a 'Quantum Sequential Growth' model, or QSG, by using the language of measure theory [19][20]. While we won't go into the full details of measure theory here, the rough idea is presented as the following.

Measure theory relies on a sample space of possible configurations Ω, which in this case would be the space of all past-finite causets. A set, called the σ-algebra $\Sigma(\Omega)$, is defined as the collection of subsets of Ω that include the empty set $\emptyset$ and Ω itself, and is closed under the complement operation and under countable unions.

A classical measure theory then has a classical measure μ_c which takes an element of $\Sigma(\Omega)$ and assigns to it a real value, which we conceptualise as a classical probability that satisfies the third Kolmogorov axiom of measure theory

$$\mu_c(\alpha \cup \beta) = \mu_c(\alpha) + \mu_c(\beta) \tag{2.8}$$

for $\alpha, \beta \in \Sigma(\Omega)$. However, with quantum measure theory for a quantum measure μ, this axiom is relaxed in favour of the quantum sum rule

$$\mu(\alpha \cup \beta \cup \gamma) = \mu(\alpha \cup \beta) + \mu(\beta \cup \gamma) + \mu(\gamma \cup \alpha) - \mu(\alpha) - \mu(\beta) - \mu(\gamma) \tag{2.9}$$

for $\alpha, \beta, \gamma \in \Sigma(\Omega)$ which must always be satisfied.

While there has been a lot of work on QSG, it is an area that remains relatively unexplored compared to the more fleshed out parts of CST, particularly with regards to the space of causets that QSG models can produce [9].

2.5.3 Sum-over-histories

An intermediate theory of quantum causet dynamics between the microscopic dynamics of quantum sequential growth and the continuum classical dynamics of the EFE could prove to be useful when working with large causets. There are two ways we can formalise this theory; using the Hamiltonian approach or the Lagrangian approach. The Hamiltonian approach is a lot more unnatural when used with causets, as it creates an unphysical distinction between space and time which does not exist at the causet level. This intermediate dynamics could instead be based on the Lagrangian approach, given by a sum-over-histories achieved by summing quantum amplitudes over the space of causets Ω which gives the partition function

[21]

$$Z = \sum_{\mathcal{C} \in \Omega} e^{iS[\mathcal{C}]} \tag{2.10}$$

where $S[\mathcal{C}]$ is a causal set action for the causal set $\mathcal{C}$. First, we must construct a causet action which we expect to limit to the Einstein-Hilbert action in the continuum. In the next chapter, we outline efforts to find such an action.

Chapter 3

Causal Set Action

In order to formulate an intermediate sum-over-histories dynamics as explored in Section 2.5.3, we require a causal set action, $S(\mathcal{C})$. As this is an intermediate dynamics, we expect this action to approach the Einstein-Hilbert action (Eq. A.1) in the continuum limit.

In this chapter we derive the Benincasa-Dowker-Glaser (BDG) action starting with the d'Alembertian of a scalar field on the causal set.

3.1 Causet d'Alembertian

When trying to define a differential operator on a discrete spacetime, we face an obvious issue in the fact that this cannot be done at a single element; on any continuous manifold, any derivative is defined as the limit of a quantity between two points. Analogously, on a discrete manifold, we can imagine that the 'closest' elements play a key role in the definition of a differential operator, which while non-local in a sense may tend towards locality in the continuum limit. However, consider the hyperboloid defined by one Planck unit of proper time away from a causet element x in a causet that has been faithfully embedded in Minkowski space. This hyperboloid stretches towards infinity in both the future and past directions, and the elements in the vicinity of this surface are connected to x by links. These can be considered to be the 'nearest neighbours' of x. It is easy to see how there an infinite number of these nearest neighbours, which poses a problem for any sense of 'discrete locality' as explained by Sorkin [22]. This radical non-locality poses a problem when trying to define a field theory on the causet; if this non-locality cannot be tamed, we are left without a d'Alembertian, which is crucial to defining, for example, the equation of

motion for a massless real scalar field ϕ which is expected to be $\partial^2\phi = g_{\mu\nu}\partial^\mu\partial^\nu\phi = 0$ in the continuum limit. How this non-locality can be tackled, and how it manifests at different scales is discussed at length by Sorkin [22].

3.1.1 Discretising the d'Alembertian

The approach taken by Sorkin [22] follows from the discretisation of a derivative, whereas the approach taken by Henson [23] is based around finding an intermediate d'Alembertian analogue on the continuum that encodes non-locality, and discretising that. Here, we will summarise Sorkin's approach. Consider a real scalar function $\phi(t)$ for $t \in \mathbb{R}$. If we discretise the domain of the function as a lattice with spacing Δt, as is required in computational methods, we can estimate the second derivative of ϕ with respect to t as

$$\frac{\partial^2\phi}{\partial t^2}(t) \approx \frac{1}{\Delta t^2}\left(\phi(t+\Delta t) - 2\phi(t) + \phi(t-\Delta t)\right) \tag{3.1}$$

Analogising this to a 2D d'Alembertian for causal sets, we can consider a real scalar field ϕ on a causal set $\mathcal{C}$, such that it maps every causet element to a real scalar, i.e. $\phi : \mathcal{C} \to \mathbb{R}$. For a causet, the length scale Δt would become the fundamental causet length scale l. Then, we require the causet d'Alembertian to be causal in the sense that it can only involve elements in the past. In this effort, we define past 'layers': sets $L_k(y)$ that form the past k-nearest neighbours to a causet element y: $L_k(y) = \{x \in \mathcal{C} : x \prec y,\ n(x,y) = k-1\}$. This indicates how many links away a certain element is, and therefore roughly how much 'further away' it is physically.

3.1.2 2D and 4D causet d'Alembertians

The 2D causet d'Alembertian is then

$$\hat{B}^{(2)}\phi(x) = \frac{4}{l^2}\left(-\frac{1}{2}\phi(x) + \left(\sum_{y\in L_1(x)} -2\sum_{y\in L_2(x)} + \sum_{y\in L_3(x)}\right)\phi(y)\right) \tag{3.2}$$

which is found to limit to the 2D d'Alembertian on the continuum. This result was then extended to the 4D case by Benincasa and Dowker [10][21]

$$\hat{B}^{(4)}\phi(x) = \frac{4}{\sqrt{6}l_p^2}\left(-\phi(x) + \left(\sum_{y\in L_1(x)} -9\sum_{y\in L_2(x)} +16\sum_{y\in L_3(x)} -8\sum_{y\in L_4(x)}\right)\phi(y)\right) \tag{3.3}$$

and to various other dimensions by Dowker and Glaser [24].

3.1.3 Continuum limit

Does this discrete d'Alembertian give the expected result in the continuum? Consider a real scalar test field ϕ on $\mathcal{M} = \mathbb{M}^4$. By sprinkling this manifold at density $\rho = l^{-4}$, we generate a causet $\mathcal{C}(\mathcal{M}, \rho)$. The real scalar field can be translated to the causet by identifying its value at the spacetime events associated with the causet elements, with the sprinkled causet elements; we call this causet real scalar field ϕ as well, and we label a spacetime event x the same as its causet element analogue, in a minor abuse of notation (note: this means we require that x is one of the points that become causet elements in the sprinkling process). Now, $\hat{\mathbf{B}}^{(4)}\phi$ is the random variable associated with the discrete d'Alembertian applied to the randomly generated causet. By taking the Poisson distribution, we can then write the mean of this random variable at a point $x \in \mathcal{M}$

$$\langle \hat{\mathbf{B}}^{(4)}\phi(x)\rangle = 4\sqrt{\frac{\rho}{6}}\left[-\phi(x) + \rho\int_{y\in J^-(x)} \mathrm{d}^4y\phi(y)e^{-\rho V_{xy}}\left(1 - 9\rho V_{xy} + 8\left(\rho V_{xy}\right)^2 - \frac{4}{3}\left(\rho V_{xy}\right)^3\right)\right] \tag{3.4}$$

where V_{xy} is the volume of the causal interval between x and y. Benincasa and Dowker found that this limited to the continuum value in the limit of $\rho \to \infty$,

$$\lim_{\rho\to\infty}\langle \hat{\mathbf{B}}^{(4)}\phi(x)\rangle = \partial^2\phi(x) \tag{3.5}$$

as was required for a sensible discrete d'Alembertian. An extension to this is to find the continuum limit for the 4D causet action for a sprinkling of a general curved manifold $\mathcal{M}$, not just the flat space. This is achieved simply by including the factor $\sqrt{-g}$ in the volume measure of the y integral in Eq. 3.4. Benincasa and Dowker found that

$$\lim_{\rho\to\infty}\langle \hat{\mathbf{B}}^{(4)}\phi(x)\rangle = \left(\partial^2 - \frac{1}{2}R(x)\right)\phi(x) \tag{3.6}$$

where $R(x)$ is the Ricci curvature scalar at x.

3.2 Benincasa-Dowker-Glaser Action

We will now make use of the results in the previous section to construct a d-dimensional causet action as formulated by Benincasa, Dowker and Glaser (BDG). First, we construct the d-dimensional d'Alembertian as calculated by Dowker and Glaser [24][25]. Let $\mathcal{C}$ be a causet well-approximated by a d-dimensional Lorentzian manifold $\mathcal{M}$, with a real scalar field $\phi : \mathcal{C} \to \mathbb{R}$ defined on it. The d-dimensional causet d'Alembertian at x is then

$$\hat{B}^{(d)}\phi(x) = \frac{1}{l^2}\left(\alpha_d \phi(x) + \beta_d \sum_{i=1}^{n_d} C_i^{(d)} \sum_{y \in L_i(x)} \phi(y)\right) \tag{3.7}$$

where α_d, β_d, n_d and $C_i^{(d)}$ are constants given for all d in [25] and also in Appendix B for convenience. We find that the mean of the random variable associated with computing this d'Alembertian at an element $x \in \mathcal{C}(\mathcal{M}, \rho)$ in a causet generated by sprinkling $\mathcal{M}$ at density $\rho = l^{-d}$, in the limit of $\rho \to \infty$, becomes [21]

$$\lim_{\rho \to \infty} \langle \hat{\mathbf{B}}^{(d)} \phi(x) \rangle = \left(\partial^2 - \frac{1}{2}R(x)\right)\phi(x) \tag{3.8}$$

where, as in the previous section, x is identified both with a causet element and the spacetime point from whence it came, and similarly with ϕ.

3.2.1 Scalar curvature of a causet

This expression can then be inverted as done by Benincasa and Dowker [10], by applying $\phi(x) = -2$ as the test scalar field to find the Ricci scalar curvature estimator of a causal set

$$R(x) = -\frac{2}{l^2}\left(\alpha_d + \beta_d \sum_{i=1}^{n_d} C_i^{(d)} |L_i(x)|\right) \tag{3.9}$$

where $|L_i(x)|$ is the cardinality of $L_i(x)$.

3.2.2 The action

The scalar curvature can then be summed over all the elements of a causal set, with normalisations defined such that the continuum approximation can give us the Einstein-Hilbert action, to find the BDG action for a dimension $d \in \mathbb{N}$, $d > 1$

$$\begin{aligned}\frac{1}{\hbar}S^{(d)}_{\mathrm{BDG}}(\mathcal{C}) &= \frac{l^d}{2l_p^{d-2}}\sum_{x\in\mathcal{C}}R(x)\\ &= -\left(\frac{l}{l_p}\right)^{d-2}\left(\alpha_d N - \beta_d\sum_{i=1}^{n_d}C_i^{(d)}N_i\right)\\ &= \zeta_d\left(N + \frac{\beta_d}{\alpha_d}\sum_{i=1}^{n_d}C_i^{(d)}N_i\right)\end{aligned} \tag{3.10}$$

where $\zeta_d = -\alpha_d(l/l_p)^{d-2}$, N is the cardinality of $\mathcal{C}$ and N_i is the number of order intervals of cardinality $(i+1)$ in $\mathcal{C}$.

For 2D, this action is

$$\frac{1}{\hbar}S^{(d)}_{\mathrm{BDG}}(\mathcal{C}) = N - 2N_1 + 4N_2 - 2N_3 \tag{3.11}$$

and for 4D, it is

$$\frac{1}{\hbar}S^{(d)}_{\mathrm{BDG}}(\mathcal{C}) = \frac{4l^2}{\sqrt{6}l_p^2}\left(N - N_1 + 9N_2 - 16N_3 + 8N_4\right) \tag{3.12}$$

3.2.3 Suppression of bilayer causets

An analytic result from Loomis and Carlip [26] showed that the class of bilayer causets was suppressed by the BDG action in the sum-over-histories. While there is further work that needs to be done to show that the rest of the non-manifold-like causets can be suppressed in the macroscopic limit (particularly for the KR causets which form the class which is by far the most dominant in the space), this is an encouraging result as the bilayer causets form a larger class than the those of manifold-like causets, yet are suppressed by the BDG action.

3.3 Continuum limit of the BDG action

In the continuum limit, we expect the BDG action to give us the EH action; after all, it has been specifically constructed with that in mind. However Benincasa et al. [27] found that the action would not vanish in the continuum limit when evaluated over a sprinkled flat causal interval $A(p,q) \subset \mathbb{M}^2$, instead limiting to a constant term related to the boundary.

An argument for why this boundary term is to be expected was given by Dowker [28]. This argument rests on the nature of the construction of the BDG action; it is retarded

in the sense that the scalar curvature estimator it is based on counts over the preceding elements of a given causet element. Given a causet element **not** on, or very near to, the past boundary, there are generally enough preceding elements (due to the incredibly high density of points) for the required contributions to result in the scalar curvature estimator limiting to the Ricci scalar in the continuum, and thus giving us the EH contribution.

However we can construct an *advanced* BDG action similar to the one already constructed, except based around an advanced scalar curvature estimator with sums over *succeeding* elements: e.g. we sum over the layers defined for elements to the future of the element being considered. However this will give us the exact same result for the BDG action, as seen simply from the definition in Eq. 3.10 which is invariant under order reversal. Therefore we expect elements **not** on (or very near to) the future boundary to give the correct contribution, and this includes the past boundary.

Considering these two arguments, most elements embedded in the manifold give the correct contribution to the action in the limit. However, the elements not covered by these arguments are the ones in the immediate vicinity of the intersection of these two boundaries. These don't have enough 'space' either in their future on in their past, and thus the lack of elements will interfere with the limit of the scalar curvature estimator in this intersection. Thus these elements give rise to a boundary term - the exact form of which forms the basis of the next chapter.

Chapter 4

Benincasa-Dowker Conjecture

In this chapter we explore a conjecture regarding the continuum limit of the BDG action and provide some new evidence for it.

4.1 The random discrete action and the conjecture

In the previous chapter, we found that boundary terms are expected to arise in the continuum limit of the BDG action. This leads to a conjecture based on the relationship that the BDG action has to the EH action. Consider a finite volume globally hyperbolic Lorentzian manifold $\mathcal{M}$ of dimension d. The boundary $\partial\mathcal{M}$ is then achronal, i.e. it consists of only spacelike and null parts, and none of it is timelike. We can split up this boundary into two parts, $\partial\mathcal{M} = \Sigma_- \cup \Sigma_+$, where Σ_- is the 'past boundary' where all past-directed timelike curves must intersect with when leaving $\mathcal{M}$, and vice versa for Σ_+.

We can then sprinkle $\mathcal{M}$ at density ρ to generate a causet $\mathcal{C}$. We can then evaluate the BD action on this sprinkled causet, giving us a random variable $\mathbf{S}_\rho(\mathcal{M})$ which we refer to as the random discrete action.

The exact form of the relationship between the continuum limit of the random discrete action and the EH action was conjectured by Benincasa and Dowker [21] to be

$$\lim_{\rho\to\infty} \frac{1}{\hbar}\langle \mathbf{S}_\rho(\mathcal{M})\rangle = \frac{1}{l_p^{d-2}}\left(\frac{1}{2}\int_{\mathcal{M}} \mathrm{d}^d x\sqrt{-g}R + \mathrm{Vol}_{d-2}(J)\right) \tag{4.1}$$

where R is the Ricci curvature scalar and $\mathrm{Vol}_{d-2}(J)$ is the $(d-2)$-volume of $J = \Sigma_- \cap \Sigma_+$, the intersection of the past and future boundaries of the manifold.

The latter quantity is a boundary term that arises due to divergences at the boundaries, and the region J is referred to as the joint.

The LHS of the conjecture is the mean of the random discrete action of a causal set achieved by sprinkling $\mathcal{M}$ at a density ρ. This quantity is

$$\frac{1}{\hbar}\langle \mathbf{S}_\rho(\mathcal{M})\rangle = \zeta_d \left(\langle \mathbf{N}_\rho(\mathcal{M})\rangle + \frac{\beta_d}{\alpha_d} \sum_{i=1}^{n_d} C_i^{(d)} \langle \mathbf{N}_{i,\rho}(\mathcal{M})\rangle \right) \tag{4.2}$$

where $\mathbf{N}$ is the random variable associated with the cardinality of the causal set, and $\mathbf{N}_i$ is the random variable of the number of order intervals of cardinality $(i+1)$ in the causal set. Via the Poisson distribution, we can express these means explicitly to find the LHS of Eq. 4.1

$$\begin{aligned} \text{LHS} &= \lim_{\rho\to\infty} \frac{1}{\hbar}\langle \mathbf{S}_\rho(\mathcal{M})\rangle \\ &= \lim_{\rho\to\infty} \zeta_d \left(\rho \int_{\mathcal{M}} \mathrm{d}V + \frac{\beta_d}{\alpha_d} \sum_{i=1}^{n_d} C_i^{(d)} \rho^2 \iint_{\substack{\mathcal{M}\times\mathcal{M} \\ q\in J^+(p)}} \mathrm{d}V_p \mathrm{d}V_q \frac{(\rho V_{pq})^{i-1}}{(i-1)!} e^{-\rho V_{pq}} \right) \end{aligned} \tag{4.3}$$

where V_{pq} is the volume of the Alexandrov interval between points p and q on $\mathcal{M}$, and $J^+(p)$ is the causal future of p (see App. A). For the rest of this chapter it is important to be careful to distinguish between the point p and the sprinkling density ρ.

4.2 Evidence for the conjecture in the literature

While this conjecture is lacking a formal proof, there are many pieces of evidence for it in the literature. All these pieces of evidence are based on choosing a certain shape of manifold such that the manifold is globally hyperbolic, and calculating the mean of the random discrete action on the given manifold. As stated in the previous chapter, one of the first pieces of evidence for this conjecture was the 2D flat causal interval [21][27], which we will frequently refer to as a causal diamond due to its shape. This was then extended to the flat space causal diamond in all dimensions [29]. Further evidence in 2D flat space has also manifested in the form of a 'null triangle', a 'null cylinder' [27] and a 'slab' cylinder [28].

Dowker then extended the results of the 2D causal diamond, slab cylinder, null triangle, and the 4D causal diamond to include a specific kind of curvature [28]. This curvature was expressed in the form of a specific conformal factor. Machet and Wang then extended the

result of a small (such that Riemann normal coordinates can be used) causal diamond to a case with arbitrary curvature, in all dimensions, finding that the BDG is well behaved on those spacetimes [30]. More recently, they gave evidence for the conjecture for a case where the 4D causal diamond was intersected by a Rindler causal horizon [31].

We now turn our attention to original results providing further evidence for the BD conjecture; namely for spacetimes which we will call the 2D flat trapezium, 2D curved trapezium, 2D flat overlapping causal diamonds, 4D flat cone and 4D curved cone.

4.3 Further evidence

This work primarily follows on from work done by Dowker [28]. The examples consist of different 2D and 4D Lorentzian manifolds on which the LHS and RHS of the conjecture is evaluated.

4.3.1 2D set up

The setup for the 2D examples closely follows the method outlined by Dowker [28]. Taking a length scale $l \sim l_p$, in 2D $\zeta_2 = -\alpha_2$ and $n_2 = 3$. In order to calculate the LHS of the conjecture as described in Eq. 4.3, we decide to split up the double integral such that the $q \in J^+(p)$ integral is calculated first, as follows

$$\begin{aligned}
\frac{1}{\hbar}\langle \mathbf{S}_\rho(\mathcal{M})\rangle &= -\alpha_2\rho\int_{\mathcal{M}} \mathrm{d}V + \beta_2\sum_{i=1}^{3} C_i^{(2)}\rho^2 \int_{\mathcal{M}} \mathrm{d}V_p \int_{\substack{\mathcal{M}\\ q\in J^+(p)}} \mathrm{d}V_q \frac{(\rho V_{pq})^{i-1}}{(i-1)!} e^{-\rho V_{pq}} \\
&= \int_{\mathcal{M}} \mathrm{d}V \left(-\alpha_2\rho + \beta_2\sum_{i=1}^{3} C_i^{(2)}\rho^2 \int_{\substack{\mathcal{M}\\ q\in J^+(p)}} \mathrm{d}V_q \frac{(\rho V_{pq})^{i-1}}{(i-1)!} e^{-\rho V_{pq}} \right) \\
&= \int_{\mathcal{M}} \mathrm{d}V_p L_\rho(p)
\end{aligned} \tag{4.4}$$

where we have defined a new function, $L_\rho(p)$, which is integrated over the entire manifold. This function should tend to $R/2$ on the manifold, and can diverge on the boundary. This divergence on the boundary produces the extra joint term in the Benincasa-Dowker conjecture.

It is simpler to evaluate this expression by differentiating under the integral. By defining the $i = 1$ term of the sum as

$$I(p) = \int_{\substack{\mathcal{M} \\ q \in J^+(p)}} \mathrm{d}V_q e^{-\rho V_{pq}} \tag{4.5}$$

and introducing a differential operator

$$\hat{O} = C_1^{(2)} - \rho C_2^{(2)} \partial_\rho + \frac{1}{2}\rho^2 C_3^{(2)} \partial_\rho^2 \tag{4.6}$$

we can recover $L_\rho(p)$ via the expression

$$L_\rho(p) = -\alpha_2 \rho - \beta_2 \rho^2 \hat{O} I \tag{4.7}$$

and thus the LHS is given by

$$\mathrm{LHS} = \lim_{\rho \to \infty} \int_{\mathcal{M}} \mathrm{d}V_p L_\rho(p) \tag{4.8}$$

As given in Appendix B and [25], the coefficients $\alpha_2 = -2$, $\beta_2 = 4$ and $C_i^{(2)} = (1, -2, 1)$. The differential operator $\hat{O}$ is then

$$\hat{O} = 1 + 2\rho\partial_\rho + \frac{1}{2}\rho^2 \partial_\rho^2 \tag{4.9}$$

and

$$L_\rho(p) = 2\rho - 4\rho^2 \hat{O} I \tag{4.10}$$

for the 2D examples.

4.3.2 2D flat trapezium

We take $\mathcal{M}$ to be a trapezium in $\mathbb{M}^2$, bounded by null boundaries on the sides and two spacelike boundaries at the top and bottom. The construction is similar to the 2D triangle in [28] but with the limits of integration on the p integral spanning from $t = a$ to $t = T$ rather than $t = 0$ to $t = T$. The shape is seen in Fig. 4.1.

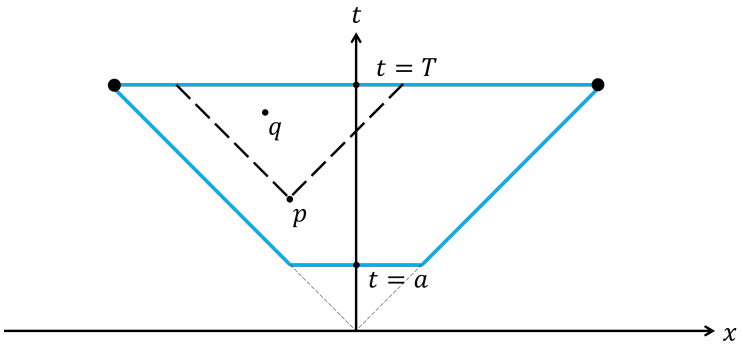

Figure 4.1: A trapezium in flat, Minkowski space defined by limits $t = a$ to $t = T$, and $x = -t$ to $x = t$, marked by the blue boundary. The region for the q integration at a point $p \in \mathcal{M}$ is also shown. The joint $J = \Sigma_- \cap \Sigma_+$ consists of the two marked points at $t = T$, $x = \pm T$.

As this is flat space with $R = 0$ everywhere, the Einstein-Hilbert term on the RHS of Eq. 4.1 vanishes, leaving only the term for the volume of the joint. As the joint for this 2D trapezium is the same as that for the triangle - the two points labelled in Fig. 4.1 - the volume, and therefore the entire RHS, is simply 2. If the conjecture holds for this manifold, we expect the LHS of Eq. 4.1, evaluated on the trapezium, to be equal to this value.

In order to evaluate $I(p)$, we find that it is simpler to transform to null coordinates centred on the point p. By taking $\Delta^\mu = q^\mu - p^\mu$, we define u and v as

$$u = \frac{1}{\sqrt{2}}(\Delta^0 - \Delta^1) \qquad\qquad v = \frac{1}{\sqrt{2}}(\Delta^0 + \Delta^1) \tag{4.11}$$

and find that, as $\tau_{pq} = -\eta_{\mu\nu}\Delta^\mu\Delta^\nu = 2uv$, the volume of the causal interval between p and q takes a simple form as $V_{pq} = uv$.

By defining $Q = \sqrt{2}(T - t)$, we find that the limits of the region for the q integral are, in these null coordinates, $u = 0$ to $u = Q$ and $v = 0$ to $v = Q - u$. We write

$$I(p) = \int_0^Q \mathrm{d}u \int_0^{Q-u} \mathrm{d}v e^{-\rho uv} = \int_0^Q \mathrm{d}u \frac{(1 - e^{-\rho u(Q-u)})}{\rho u} \tag{4.12}$$

and we can differentiate under the integral as v is independent of ρ

$$\partial_\rho I = \int_0^Q \mathrm{d}u \left(\frac{(Q-u)}{\rho} e^{-\rho u(Q-u)} - \frac{1 - e^{-\rho u(Q-u)}}{\rho^2 u} \right) \tag{4.13}$$

$$\partial_\rho^2 I = \int_0^Q \mathrm{d}u \left(2\frac{(1-e^{-\rho u(Q-u)})}{\rho^3 u} - 2\frac{(Q-u)}{\rho^2} e^{-\rho u(Q-u)} - \frac{u(Q-u)^2}{\rho} e^{-\rho u(Q-u)} \right) \tag{4.14}$$

The above results allow us to put together $\hat{O}I$, which is

$$\hat{O}I = -\frac{1}{2}\int_0^Q \mathrm{d}u(Q-u)(\rho u(Q-u)-2)e^{-\rho u(Q-u)} \tag{4.15}$$

and this is inserted into Eq. 4.10 to find

$$\begin{aligned} L_\rho(p) &= 2\rho + 2\rho^2 \int_0^Q \mathrm{d}u(Q-u)(\rho u(Q-u)-2)e^{-\rho u(Q-u)} \\ &= 2\rho + \frac{1}{4}\rho^2 Q \left(\frac{1}{\sqrt{\rho}} \left(\sqrt{\pi} e^{-\frac{\rho Q^2}{4}} (\rho Q^2 - 6) \mathrm{erfi}\left(\frac{\sqrt{\rho} Q}{2} \right) \right) - 2Q \right) \end{aligned} \tag{4.16}$$

As $L_\rho(p)$ is independent of t, we can evaluate the t integral independently,

$$\int_{\mathcal{M}} \mathrm{d}V_p = \int_a^T \mathrm{d}t \int_{-t}^t \mathrm{d}x = 2\int_a^T t\mathrm{d}t \tag{4.17}$$

which allows us to evaluate the LHS of the Benincasa-Dowker conjecture

$$\begin{aligned} \mathrm{LHS} = \lim_{\rho\to\infty} 2\int_a^T t\mathrm{d}t L_\rho(p) = \lim_{\rho\to\infty} \Big[&-2a^2\rho - \sqrt{2\pi\rho} e^{-\frac{1}{2}\rho(T-a)^2} (a^3\rho \\ &- T(2a^2\rho+1) + aT^2\rho) \mathrm{erfi}\left(\sqrt{\frac{\rho}{2}}(T-a) \right) + 2aT\rho \Big] \end{aligned} \tag{4.18}$$

The imaginary error function can be transformed into the Dawson function,

$$\mathrm{erfi}(x) = \frac{2}{\sqrt{\pi}} e^{x^2} F(x) \tag{4.19}$$

which has a well defined expansion as $x \to \infty$,

$$\lim_{x\to\infty} F(x) = \lim_{x\to\infty} \frac{1}{2x} + \frac{1}{4x^3} + \frac{3}{8x^5} + ... \tag{4.20}$$

Returning to the LHS of the conjecture and rewriting in terms of the Dawson function and then the first two terms of its expansion at infinity we find

$$
\begin{aligned}
\text{LHS} &= \lim_{\rho\to\infty}\left[-2a^2\rho - 2\sqrt{2\rho}(a^3\rho - T(2a^2\rho+1) + aT^2\rho)F\left(\sqrt{\frac{\rho}{2}}(T-a)\right) + 2aT\rho\right] \\
&= \lim_{\rho\to\infty}\left[- 2a^2\rho - 2\sqrt{2\rho}(a^3\rho - T(2a^2\rho+1) + aT^2\rho)\left(\frac{1}{\sqrt{2\rho}(T-a)} + \frac{1}{\sqrt{2\rho^3}(T-a)^3}\right)\right. \\
&\quad \left. + 2aT\rho\right] \\
&= \lim_{\rho\to\infty}\left[\frac{2\rho(a-T)^3 - 2T}{\rho(a-T)^3}\right] \\
&= 2
\end{aligned}
\tag{4.21}
$$

As the LHS = RHS, which is the volume of the joint, the BD conjecture holds for this case.

4.3.3 2D trapezium with curvature

This example is identical to the trapezium shape shown in Fig. 4.1 but with curvature. This curvature will be expressed via a conformal factor $\Phi(t) \equiv (1 - bt^2)$ for a conformally flat metric

$$
\mathrm{d}s^2 = \Phi(t)^2\eta_{\mu\nu}\mathrm{d}x^\mu\mathrm{d}x^\nu = \Phi(t)^2(-\mathrm{d}t^2 + \mathrm{d}x^2) \tag{4.22}
$$

We will only consider the case of a small curvature parameter b, assuming that the Ricci curvature scalar $R = 4(d-1)b = 4b$ is approximately constant over the entire region of integration and retaining only the terms that are linear in b. This assumption is equivalent to the size of the region $\mathcal{M}$ being small in comparison to the radius of curvature.

First, we calculate the RHS of Eq. 4.1. The volume of the joint is the same as in the flat case, as the curvature does not affect the volume of a 0-sphere, however this time we have a non-zero Einstein-Hilbert term. In order to calculate this term, we first need the determinant of the metric. We find that $\sqrt{-g} = \Phi(t)^2 = (1 - bt^2)^2$, and thus, after keeping only linear terms in b, we find

$$
\frac{1}{2}\int_{\mathcal{M}} \mathrm{d}^d x\sqrt{-g}R = 2b\int_a^T \mathrm{d}t\int_{-t}^{t}\mathrm{d}x = 2b(T^2 - a^2) \tag{4.23}
$$

giving us the result RHS $= 2b(T^2 - a^2) + 2$.

The derivation for $L_\rho(p)$ follows a similar procedure to the flat case, but with only linear terms in b. We arrive at [28]

$$\begin{aligned}L_\rho(p) = 2\rho + \frac{\rho Q}{24}\Bigg[&bQ\Big(24\rho t^2(\rho Q^2-5) + 24\rho Q t(\rho Q^2-6) + 7\rho Q^2(\rho Q^2-8) - 3\Big)\\&+ 24bt - 24\rho Q\Bigg] - \frac{\sqrt{\rho}}{12\sqrt{2}}F\left(\sqrt{\frac{\rho}{2}}Q\right)\Bigg[bQ\Big(24\rho t^2(\rho Q^2(\rho Q^2-6)+3)\\&+ 24\rho Q t(\rho Q^2(\rho Q^2-7)+5) + \rho Q^2(7\rho Q^2(\rho Q^2-9)+39) - 3\Big)\\&+ 24bt - 24\rho Q(\rho Q^2-3)\Bigg]\end{aligned} \tag{4.24}$$

where $Q = T - t$. Integrating this over $\mathcal{M}$ and dropping quadratic and higher order terms in b we find

$$\begin{aligned}\text{LHS} &= \lim_{\rho\to\infty}\int_{\mathcal{M}} \mathrm{d}^2p(1-bt^2)^2 L_\rho(p) = \lim_{\rho\to\infty}\int_a^T \mathrm{d}t\int_{-t}^t \mathrm{d}x(1-bt^2)^2 L_\rho(p)\\
&= \lim_{\rho\to\infty}\Bigg[-\frac{1}{24\rho(T-a)^2}\Bigg[15\Big(7a^4b\rho - 28a^3b\rho T + a^2(90b\rho T^2 - 3b + 8\rho)\\
&\quad - 2aT(62b\rho T^2 - 3b + 8\rho) + T^2(55b\rho T^2 - 11b + 8\rho)\Big)\,{}_2F_2\left(1,1;-\frac{5}{2},2;-\frac{1}{2}\rho(T-a)^2\right)\\
&\quad - 6\Big(2a^4\rho(21b+2\rho) - 8a^3\rho T(21b+2\rho) + a^2(4\rho T^2(125b+6\rho) - 15b + 40\rho)\\
&\quad - 8a\rho T^3(83b+2\rho) + 10aT(3b-8\rho)\\
&\quad + T^2(2\rho T^2(145b+2\rho) - 55b + 40\rho)\Big)\,{}_2F_2\left(1,1;-\frac{3}{2},2;-\frac{1}{2}\rho(T-a)^2\right)\\
&\quad + \Big(a^4\rho(111b+40\rho) - 4a^3\rho T(111b+40\rho) + a^2(2\rho T^2(733b+120\rho) - 45b + 120\rho)\\
&\quad - 4a\rho T^3(511b+40\rho) + 30aT(3b-8\rho) + \rho T^4(911b+40\rho)\\
&\quad + 15T^2(8\rho - 11b)\Big)\,{}_2F_2\left(1,1;-\frac{1}{2},2;-\frac{1}{2}\rho(T-a)^2\right) + 2\sqrt{2\rho}T(T-a)^2\Big(b\rho^3(31a^2\\
&\quad - 62aT + 55T^2)(a-T)^4 - 3\rho^2(T-a)^2(39a^2b - 78abT + 71bT^2 + 8)\\
&\quad + 3\rho(b(-7a^2 + 14aT + T^2) + 8) - 93b\Big)F\left(\sqrt{\frac{\rho}{2}}(T-a)\right)\\
&\quad - 2\rho(a-T)^3\Big(2b\rho T^3(105a^2\rho - 79) + 4ab\rho T^2(43 - 31a^2\rho) + bT(a^2\rho(31a^2\rho - 86) - 69)\\
&\quad - 172ab\rho^2T^4 - 24ab + 55b\rho^2T^5 - 24\rho T\Big)\Bigg]\Bigg]\end{aligned} \tag{4.25}$$

Where ${}_2F_2(1,1;c,2;x)$ is the generalised hypergeometric function for a constant c, and $F(x)$ is the Dawson function as seen before. By taking expansions of the $c=-5/2$,$-3/2$ and $-1/2$ hypergeometric functions in the limit of $x\to-\infty$ (as the argument of the function is proportional to $-\rho$), we find

$$\lim_{x\to-\infty}{}_2F_2\left(1,1;-\frac{1}{2},2;x\right)=\frac{1}{16x^3}\Big[24x^2\left(\ln(-x)-\psi\left(-\frac{3}{2}\right)\right)+4\sqrt{\pi x}e^x\left(8x^3-12x^2+6x+3\right)+60x-105\Big]+... \tag{4.26}$$

$$\lim_{x\to-\infty}{}_2F_2\left(1,1;-\frac{3}{2},2;x\right)=\frac{1}{48x^3}\Big[120x^2\left(\ln(-x)-\psi\left(-\frac{5}{2}\right)\right)+8\sqrt{\pi}x^{3/2}e^x\left(-8x^3+20x^2-30x+15\right)+420x-945\Big]+... \tag{4.27}$$

$$\lim_{x\to-\infty}{}_2F_2\left(1,1;-\frac{5}{2},2;x\right)=\frac{1}{240x^3}\Big[840x^2\left(\ln(-x)-\psi\left(-\frac{7}{2}\right)\right)+16\sqrt{\pi}x^{5/2}e^x\left(8x^3-28x^2+70x-105\right)+3780x-10395\Big]+... \tag{4.28}$$

where $\psi(z)=\Gamma'(z)/\Gamma(z)$ is the digamma function.

By inserting these expansions along with the expansion of the Dawson function (Eq. 4.20) into Eq. 4.25, we can construct an expansion of the LHS of the conjecture as $\rho\to\infty$. The resulting expression can be arranged such that it can be loosely expressed as a power series in terms of $(1/\rho)$, and as the limit is carefully taken we find that all terms disappear apart from the $(1/\rho)^0$ term

$$
\begin{aligned}
\text{LHS} = \lim_{\rho\to\infty} \Bigg[& a^2 b \left(-8\sqrt{2\pi} e^{-\frac{1}{2}\rho(T-a)^2} \sqrt{-\frac{1}{\rho(T-a)^2}} - 2 \right) \\
& + 2bT^2 \left(1 - 4\sqrt{2\pi} e^{-\frac{1}{2}\rho(a-T)^2} \sqrt{-\frac{1}{\rho(T-a)^2}} \right) \\
& + 16\sqrt{2\pi} abT e^{-\frac{1}{2}\rho(T-a)^2} \sqrt{-\frac{1}{\rho(T-a)^2}} + 5\left(\psi\left(-\frac{5}{2}\right) - \psi\left(-\frac{3}{2}\right) \right) \Bigg] \\
= & \, 2b(T^2 - a^2) + 5\left(\psi\left(-\frac{5}{2}\right) - \psi\left(-\frac{3}{2}\right) \right) \\
= & \, 2b(T^2 - a^2) + 2
\end{aligned}
\tag{4.29}
$$

which matches precisely with the RHS, thereby proving that, for small curvature parameter b, the conjecture holds for this case as well.

4.3.4 2D flat overlapped causal diamonds

For our final 2D example, we consider a manifold made out of two overlapping causal diamonds, as shown in Fig. 4.2.

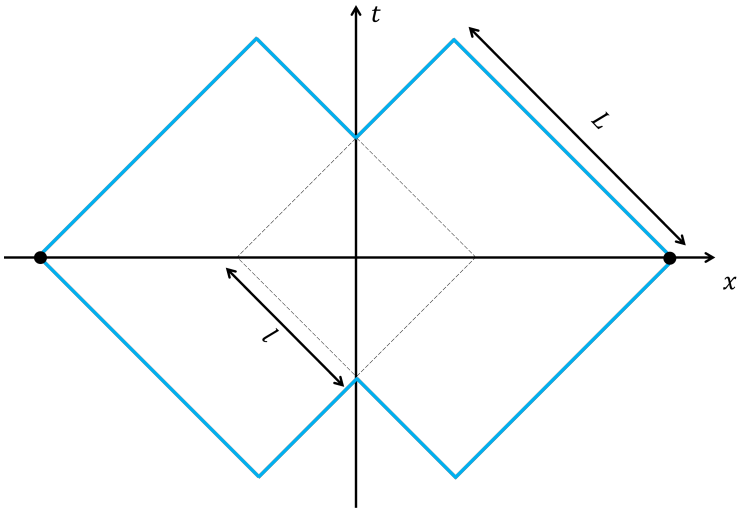

Figure 4.2: An overlapped causal diamond $\mathcal{M}$ with a null boundary. L is the length of one side of the diamond, and l is a parameter that characterises how much overlap there is. The joint is shown as the two marked points.

As with the flat trapezium, this manifold is in flat space, $\mathcal{M} \in \mathbb{M}^2$. Thus there is no contribution from the EH action and as joint is the same as the trapezium, we find that the RHS = 2. We will use null radial coordinates centred on the point p, as defined in Eq. 4.11,

for the q integration. We will also make use of capitalised null radial coordinates centred at the origin,

$$U = \frac{1}{\sqrt{2}}(t - x) \qquad\qquad V = \frac{1}{\sqrt{2}}(t + x) \tag{4.30}$$

which will be used for the p integration.

The complex nature of this shape means it is convenient to split up the manifold into regions as in Fig. 4.3.

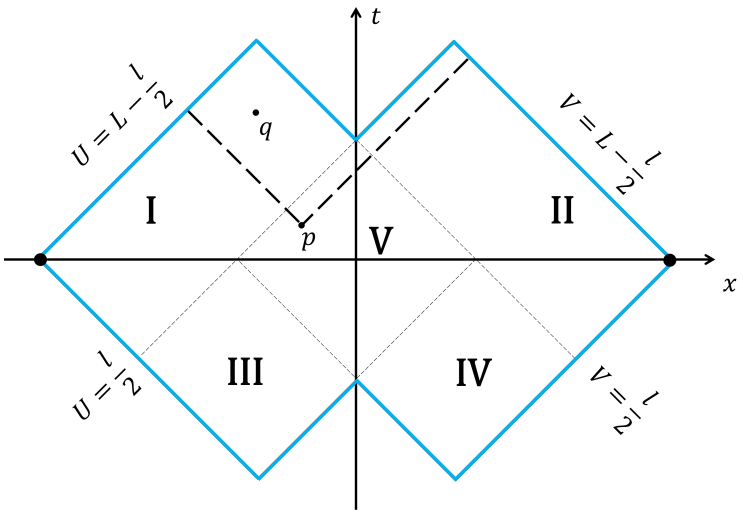

Figure 4.3: $\mathcal{M}$ split into five regions for the integration, with a point $q \in J^+(p)$ shown. The figure also shows some lines of constant U and V.

We find that the limits of integration for these regions are:

- Region I:
  - q integral: $v = [0, \frac{l}{2} - V]$, $u = [0, L - \frac{l}{2} - U]$
  - p integral: $V = [\frac{l}{2} - L, \frac{l}{2}]$, $U = [\frac{l}{2}, L - \frac{l}{2}]$
- Region II:
  - q integral: $v = [0, L - \frac{l}{2} - V]$, $u = [0, \frac{l}{2} - U]$
  - p integral: $V = [\frac{l}{2}, L - \frac{l}{2}]$, $U = [\frac{l}{2} - L, \frac{l}{2}]$
- Region III:

- q integral: $v = [0, \frac{l}{2} - V]$, $u = [0, L - \frac{l}{2} - U]$ AND $v = [\frac{l}{2} - V, L - \frac{l}{2} - V]$, $u = [0, \frac{l}{2} - U]$
- p integral: $V = [\frac{l}{2} - L, -\frac{l}{2}]$, $U = [-\frac{l}{2}, \frac{l}{2}]$

- Region IV:
  - q integral: $v = [0, L - \frac{l}{2} - V]$, $u = [0, \frac{l}{2} - U]$ AND $v = [0, \frac{l}{2} - V]$, $u = [\frac{l}{2} - U, L - \frac{l}{2} - U]$
  - p integral: $V = [-\frac{l}{2}, \frac{l}{2}]$, $U = [\frac{l}{2} - L, -\frac{l}{2}]$

- Region V:
  - q integral: $v = [0, \frac{l}{2} - V]$, $u = [0, L - \frac{l}{2} - U]$ AND $v = [\frac{l}{2} - V, L - \frac{l}{2} - V]$, $u = [0, \frac{l}{2} - U]$
  - p integral: $V = [-\frac{l}{2}, \frac{l}{2}]$, $U = [-\frac{l}{2}, \frac{l}{2}]$

The calculations for the LHS contributions from each region now follow. Taking $V_{pq} = uv$ again, we first calculate $I(p)$, then $L_\rho(p)$, then the LHS contribution for each region.

- Region I:

  Integrating $e^{-\rho uv}$ over the q integral limits for the region we find

$$\begin{aligned} I_{\mathrm{I}}(p) &= \int_0^{L-\frac{l}{2}-U} \mathrm{d}u \int_0^{\frac{l}{2}-V} \mathrm{d}v \; e^{-\rho uv} \\ &= \frac{1}{\rho}\left[\ln\left(-\frac{1}{4}\rho(l-2V)(l-2L+2U)\right) + \Gamma\left(0, -\frac{1}{4}\rho(l-2L+2U)(l-2V)\right) + \gamma\right] \end{aligned} \tag{4.31}$$

  where γ is the Euler-Mascheroni constant, and $\Gamma(s, x)$ is the upper incomplete gamma function. Then we calculate $L_{\mathrm{I}\rho}(p) = 2\rho - 4\rho^2 \hat{O} I_{\mathrm{I}}$,

$$L_{\mathrm{I}\rho}(p) = \frac{1}{2}\rho e^{\frac{1}{4}\rho(l-2V)(l-2L+2U)}\left(l^2\rho - 2l\rho(L-U+V) + 4L\rho V - 4\rho UV + 4\right) \tag{4.32}$$

  which is then integrated over Region I to find

$$\begin{aligned}\text{LHS}_{\text{I}} &= \lim_{\rho\to\infty}\left[\int_{\frac{l}{2}}^{L-\frac{l}{2}} \mathrm{d}U \int_{\frac{l}{2}-L}^{\frac{l}{2}} \mathrm{d}V L_{\text{I}\rho}(p)\right] \\ &= \lim_{\rho\to\infty}\left[2-2e^{-L\rho(L-l)}\right]\end{aligned} \tag{4.33}$$

which is the LHS contribution from Region I. We repeat this over the other four regions.

- Region II:

$$\text{LHS}_{\text{II}} = \lim_{\rho\to\infty}\left[2-2e^{-L\rho(L-l)}\right] \tag{4.34}$$

- Region III:

$$\text{LHS}_{\text{III}} = \lim_{\rho\to\infty}\left[-2e^{-l^2\rho}-2e^{-l\rho(2L-l)}-2e^{-l\rho(L-l)}+6e^{-lL\rho}+2e^{-L\rho(L-l)}-2e^{-L^2\rho}\right] \tag{4.35}$$

- Region IV:

$$\text{LHS}_{\text{IV}} = \lim_{\rho\to\infty}\left[-2\left(e^{-l^2\rho}+e^{-l\rho(2L-l)}+e^{-l\rho(L-l)}-3e^{-lL\rho}-e^{-L\rho(L-l)}+e^{-L^2\rho}\right)\right] \tag{4.36}$$

- Region V:

$$\text{LHS}_{\text{V}} = \lim_{\rho\to\infty}\left[2e^{-l^2\rho}+4e^{-l\rho(L-l)}-4e^{-lL\rho}-2\right] \tag{4.37}$$

We now sum over these contributions to find the LHS for this manifold,

$$\begin{aligned}\text{LHS} &= \lim_{\rho\to\infty}\left[2-2e^{-l^2\rho}-4e^{-l\rho(2L-l)}+8e^{-lL\rho}-4e^{-L^2\rho}\right] \\ &= 2\end{aligned} \tag{4.38}$$

which matches exactly with the RHS, and thus the conjecture holds for this case as well.

4.3.5 4D flat cone

Now consider a manifold that takes the shape of the past lightcone of a point $m \in \mathbb{M}^4$, as shown in in Fig. 4.4. The cone is oriented such that we can make use of the previously derived result of $L_\rho(p)$ for a causal interval, which can be found in [28].

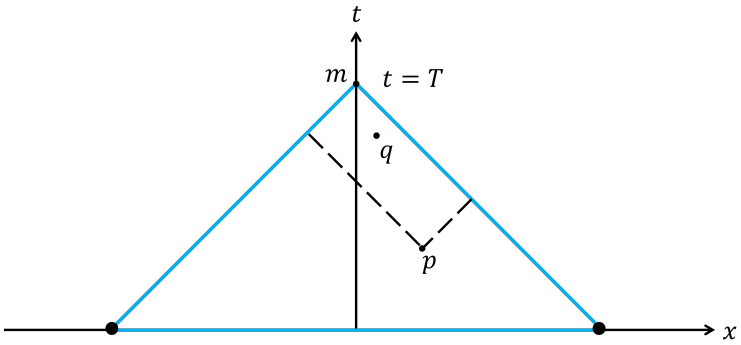

Figure 4.4: A cone in flat, 4D Minkowski space defined by limits $t = 0$ to $t = T$, and $x, y, z = -t$ to $x, y, z = t$, marked by the blue boundary. Only the x axis is shown out of the spatial axes. The region for the q integration at a point $p \in \mathcal{M}$ is also shown. The joint $J = \Sigma_- \cap \Sigma_+$ consists of the two marked points at $t = T$, $x = \pm T$.

This equivalence can be seen in Fig. 4.4. As the region where $q \in J^+(p)$ and $q \in \mathcal{M}$ is the causal interval between p and the tip of the cone at m, the q integral for this case is identical to that of the flat 4D causal diamond in [28]. $L_\rho(p)$ is therefore

$$L_\rho(p) = 2\sqrt{\frac{2\rho}{3}} e^{-\frac{1}{24}\pi\rho\tau^4} \tag{4.39}$$

where $\tau^2 = (T-t)^2 - x^2 - y^2 - z^2$ is the square of the proper time between a point $p \in \mathcal{M}$ to the tip of the cone at r.

For this flat case, again $R = 0$ and thus there is no contribution to the RHS from the EH action. The joint is a 2-sphere that exists in the $t = 0$ plane, with radius T. Therefore the volume of the joint follows the standard formula for the surface area of a sphere, and the RHS $= 4\pi T^2$.

To calculate the LHS, we now introduce null radial coordinates. These are similar to the capitalised null coordinates (the ones centred on the origin) defined in Eq. 4.30 except with the radial coordinate r (such that $r^2 = x^2 + y^2 + z^2$) taking the place of x, and we define $t' = T - t$ as the distance along t of a point p from the tip of the cone,

$$u = \frac{1}{\sqrt{2}}(t' - r) \qquad\qquad v = \frac{1}{\sqrt{2}}(t' + r) \tag{4.40}$$

which has the effect of centering the null radial coordinates at the tip of the cone. With increasing t' on the vertical axis, the diagram becomes flipped, although we can still make use of $L_\rho(p)$ for the causal diamond.

In these coordinates, $\tau^2 = 2uv$ and the volume measure becomes

$$\int_{\mathcal{M}} \mathrm{d}V_p = \frac{1}{2}\int_0^{2\pi} \mathrm{d}\phi \int_0^{\pi} \mathrm{d}\theta \iint_\sigma (u-v)^2 \mathrm{d}u\mathrm{d}v = \iint_\sigma 2\pi(u-v)^2 \mathrm{d}u\mathrm{d}v \tag{4.41}$$

where σ signifies the $u - v$ plane which is part of $\mathcal{M}$. The range of the p integral, in σ, is then shown in Fig. 4.5.

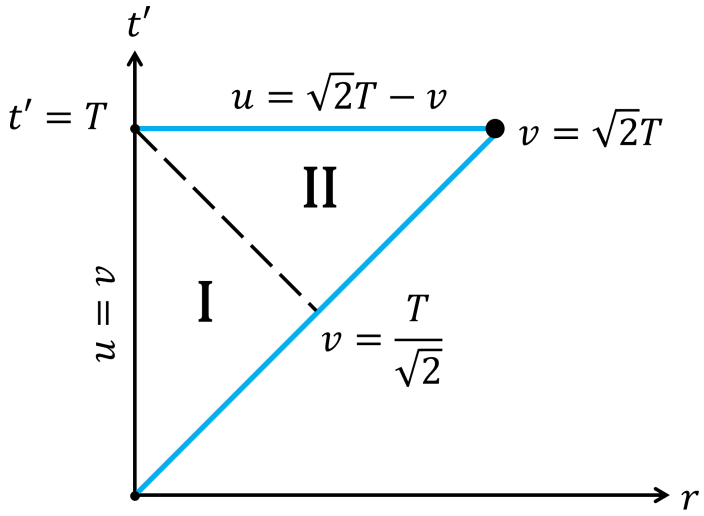

Figure 4.5: The cone shown in the $u - v$ plane. At each point on this plane, we can think of the rest of the dimensionality lying in a 2-sphere of radius $r = \frac{1}{\sqrt{2}}(v - u)$. The regions I and II indicate the two regions over which the integral is evaluated, with the limits shown as the line equations in u and v coordinates.

We find that the integration over Regions I and II give us

$$\begin{aligned}\int_{\mathcal{M}} \mathrm{d}V_p L_\rho(p) &= \left(\int_0^{\frac{T}{\sqrt{2}}} \mathrm{d}v \int_0^v \mathrm{d}u + \int_{\frac{T}{\sqrt{2}}}^{\sqrt{2}T} \mathrm{d}v \int_0^{\sqrt{2}T-v} \mathrm{d}u\right) 4\sqrt{\frac{2\rho}{3}} e^{-\frac{1}{6}\pi\rho(uv)^2}(u-v)^2 \\ &= \frac{(\pi\rho T^4 - 12)}{\rho T^2}\,\mathrm{erf}(\frac{1}{2}\sqrt{\frac{\pi\rho}{6}}T^2) \\ &\quad + 2\sqrt{\frac{6}{\rho}}\left(e^{-\frac{1}{24}\pi\rho T^4} - \ln\left(\frac{1}{24}\pi\rho T^4\right) - \Gamma\left(0, \frac{1}{24}\pi T^4\rho\right) - \gamma\right) \\ &\quad + \int_{\frac{T}{\sqrt{2}}}^{\sqrt{2}T} \frac{4}{\rho v^3}\Bigg[\left(\pi\rho v^4 + 3\right)\mathrm{erf}\left(\sqrt{\frac{\pi\rho}{6}}v\left(\sqrt{2}T - v\right)\right) \\ &\quad - \sqrt{3\rho}v e^{-\frac{1}{6}\pi\rho v^2\left(v-\sqrt{2}T\right)^2}\left(\sqrt{2}v\left(2e^{\frac{1}{6}\pi\rho v^2\left(v-\sqrt{2}T\right)^2} - 3\right) + 2T\right)\Bigg]\mathrm{d}v\end{aligned} \tag{4.42}$$

where γ is the Euler-Mascheroni constant, and $\Gamma(s,x)$ is the upper incomplete gamma function as before. As we know that

$$\lim_{x\to\infty} \mathrm{erf}(x) = 1 \tag{4.43}$$

and that $\Gamma(0,x)$ limits to

$$\lim_{x\to\infty} \Gamma(0,x) = \lim_{x\to\infty} e^{-x}\left(\frac{1}{x} - \frac{1}{x^2} + ...\right) = 0 \tag{4.44}$$

we can see that, in the limit, we are left with

$$\mathrm{LHS} = \lim_{\rho\to\infty}\left[\pi T^2 + \int_{\frac{T}{\sqrt{2}}}^{\sqrt{2}T}\left(4\pi v\ \mathrm{erf}\left(\sqrt{\frac{\pi\rho}{6}}v\left(\sqrt{2}T - v\right)\right) + \omega(v,\rho,T)\right)\mathrm{d}v\right] \tag{4.45}$$

where

$$\begin{aligned}\omega(v,\rho,T) = \frac{4}{\rho v^3}\Bigg[&3\,\mathrm{erf}\left(\sqrt{\frac{\pi\rho}{6}}v\left(\sqrt{2}T - v\right)\right) \\ &+ \sqrt{3\rho}v\left(\left(3\sqrt{2}v - 2T\right)e^{-\frac{1}{6}\pi\rho v^2\left(v-\sqrt{2}T\right)^2} - 2\sqrt{2}v\right)\Bigg]\end{aligned} \tag{4.46}$$

is a function that is integrated over $v = [T/\sqrt{2}, \sqrt{2}T]$. This function has no distributional character over these limits; we see quite trivially that there are no divergences over the range of integration, and that $\omega(v,\rho,T)$ limits to 0 everywhere in that range as $\rho\to\infty$, showing

that it does not contribute to the LHS.

Therefore,

$$\begin{aligned}\text{LHS} &= \lim_{\rho\to\infty}\left[\pi T^2 + \int_{\frac{T}{\sqrt{2}}}^{\sqrt{2}T}\left(4\pi v\ \text{erf}\left(\sqrt{\frac{\pi\rho}{6}}v\left(\sqrt{2}T - v\right)\right)\right)\,\mathrm{d}v\right] \\ &= \pi T^2 + \int_{\frac{T}{\sqrt{2}}}^{\sqrt{2}T}(4\pi v)\,\mathrm{d}v \\ &= 4\pi T^2\end{aligned} \tag{4.47}$$

which matches with the RHS, meaning that the BD conjecture holds for this case as well.

4.3.6 4D cone with curvature

This example is identical to the 4D cone but with a similar conformally flat curvature introduced as before. With the conformal factor $\Phi(t) \equiv (1 - bt^2)$, we get the metric

$$\mathrm{d}s^2 = \Phi(t)^2\eta_{\mu\nu}\mathrm{d}x^\mu\mathrm{d}x^\nu = \Phi(t)^2(-\mathrm{d}t^2 + \mathrm{d}x^2 + \mathrm{d}y^2 + \mathrm{d}z^2) \tag{4.48}$$

As before, we only consider the case of a small curvature parameter b, assuming that the Ricci curvature scalar $R = 4(d-1)b = 12b$ is approximately constant over the entire region.

First, we calculate the RHS of Eq. 4.1. As the joint is a 2-sphere that exists in the $t = 0$ hyperplane, we find that the curvature conformal factor $\Phi(t) \equiv (1 - bt^2) = 1$ along this plane and thus the volume of the joint is identical to that in the case without curvature. Therefore the RHS is the EH term plus $4\pi T^2$. The EH term is found by integrating over the entire manifold and keeping only linear terms in b. Using the null radial coordinates as in Eq. 4.40, we find

$$\begin{aligned}\frac{1}{2}\int_{\mathcal{M}}\mathrm{d}^dx\sqrt{-g}R &= \frac{1}{4}\int_0^{2\pi}\mathrm{d}\phi\int_0^{\pi}\mathrm{d}\theta\left[\int_0^{\frac{T}{\sqrt{2}}}\mathrm{d}v\int_0^{v}\mathrm{d}u + \int_{\frac{T}{\sqrt{2}}}^{\sqrt{2}T}\mathrm{d}v\int_0^{\sqrt{2}T-v}\mathrm{d}u\right](12b)(u-v)^2 \\ &= 2b\pi T^4\end{aligned} \tag{4.49}$$

giving us the result RHS $= 2b\pi T^4 + 4\pi T^2$.

The derivation for $L_\rho(p)$ is outlined in Appendix A of [28]. We arrive at

$$\begin{aligned}
L_\rho(p) = {} & 2\sqrt{\frac{2\rho}{3}}e^{-\frac{1}{24}\pi\rho\tau^4} + 6b\,\mathrm{erf}\left(\frac{1}{2}\sqrt{\frac{\pi\rho}{6}}\tau^2\right) \\
& - \frac{288bt'^2}{\pi\rho\tau^6}\,\mathrm{erf}\left(\frac{1}{2\sqrt{6}}\sqrt{\pi\rho}\tau^2\right) + \frac{72b}{\pi\rho\tau^4}\,\mathrm{erf}\left(\frac{1}{2\sqrt{6}}\sqrt{\pi\rho}\tau^2\right) \\
& + \frac{4}{5}\sqrt{\frac{2\rho}{3}}b\left(t'^2+\tau^2\right)e^{-\frac{1}{24}\pi\rho\tau^4} - \frac{1}{3}\sqrt{\frac{2\rho^3}{3}}\pi bT\tau^4(T-t')e^{-\frac{1}{24}\pi\rho\tau^4} \\
& + \frac{\sqrt{6}bt'^2}{5\pi\sqrt{\rho}\tau^4}\left(112e^{-\frac{1}{24}\pi\rho\tau^4}+128\right) + \frac{\sqrt{6}b}{5\pi\sqrt{\rho}\tau^4}\left(132e^{-\frac{1}{24}\pi\rho\tau^4}-192\right) \\
& + \frac{\pi b\rho^{3/2}}{\sqrt{6}}\left(\frac{\tau^6}{45}-\frac{t'^2\tau^4}{5}\right)e^{-\frac{1}{24}\pi\rho\tau^4}
\end{aligned} \tag{4.50}$$

where τ and t' are as defined in the previous section.

Now, keeping only the terms up to linear order in b, and using $t = T - \frac{u+v}{\sqrt{2}}$,

$$\begin{aligned}
\mathrm{LHS} = {} & \lim_{\rho\to\infty}\int_{\mathcal{M}} \mathrm{d}V_p L_\rho(p) \\
= {} & \lim_{\rho\to\infty}\iint_\sigma 2\pi(u-v)^2 L_\rho(p)\left(1-b\left(T-\frac{u+v}{\sqrt{2}}\right)^2\right)^4 \mathrm{d}u\mathrm{d}v \\
= {} & \lim_{\rho\to\infty}\iint_\sigma 2\pi(u-v)^2 L_\rho(p)\left(1-4b\left(T-\frac{u+v}{\sqrt{2}}\right)^2\right) \mathrm{d}u\mathrm{d}v \\
= {} & \lim_{\rho\to\infty}\iint_\sigma \Bigg[4\pi(u-v)^2\sqrt{\frac{2\rho}{3}}e^{-\frac{1}{6}\pi\rho u^2v^2} \\
& + 12b\pi(u-v)^2\,\mathrm{erf}\left(uv\sqrt{\frac{\pi\rho}{6}}\right) + \omega(u,v,\rho,T)\Bigg]\mathrm{d}u\mathrm{d}v
\end{aligned} \tag{4.51}$$

where $\omega(u,v,\rho,T)$ are the rest of the terms in the integrand up to linear order in b, which are separated as they are difficult to integrate over.

With the first term in the integrand in Eq. 4.51 giving a contribution LHS_1, we find it is simply the term from the flat case, i.e. the joint term $\mathrm{LHS}_1 = 4\pi T^4$ as has already been shown in the previous section. Meanwhile, the second term in the integrand can be integrated over Region I (as in Fig. 4.5) and the limit can be taken to give us

$$
\begin{aligned}
\mathrm{LHS}_{2,\mathrm{I}} &= \lim_{\rho\to\infty} 12b\pi \int_0^{\frac{T}{\sqrt{2}}} \mathrm{d}v \int_0^v \mathrm{d}u(u-v)^2 \operatorname{erf}\left(uv\sqrt{\frac{\pi\rho}{6}}\right) \\
&= \lim_{\rho\to\infty} \frac{b}{4\rho^{3/2}}\Bigg[12\sqrt{6}\rho T^2\, {}_2F_2\left(\frac{1}{2},\frac{1}{2};\frac{3}{2},\frac{3}{2};-\frac{\pi T^4\rho}{24}\right) \\
&\quad + \sqrt{\rho}\left(\pi\rho T^4-36\right)\operatorname{erf}\left(\frac{1}{2}\sqrt{\frac{\pi}{6}}\sqrt{\rho}T^2\right) \\
&\quad - \frac{2\sqrt{6}}{\pi T^2}e^{-\frac{1}{24}\pi\rho T^4}\left(-\pi\rho T^4+6e^{\frac{1}{24}\pi\rho T^4}\left(\pi\rho T^4-8\right)+48\right)\Bigg] \\
&= \frac{1}{4}b\pi T^4
\end{aligned}
\tag{4.52}
$$

and over Region II to give us

$$
\begin{aligned}
\mathrm{LHS}_{2,\mathrm{II}} &= \lim_{\rho\to\infty} 12b\pi \int_{\frac{T}{\sqrt{2}}}^{\sqrt{2}T} \mathrm{d}v \int_0^{\sqrt{2}T-v} \mathrm{d}u(u-v)^2 \operatorname{erf}\left(uv\sqrt{\frac{\pi\rho}{6}}\right) \\
&= \lim_{\rho\to\infty} \int_{\frac{T}{\sqrt{2}}}^{\sqrt{2}T} \frac{4b}{\pi\rho^{3/2}v^3}\Bigg[-\pi\sqrt{\rho}v^2\Bigg(\pi\rho v\big(-2\sqrt{2}T^3+12T^2v \\
&\quad -12\sqrt{2}Tv^2+7v^3\big)-9\Bigg)\operatorname{erf}\left(\sqrt{\frac{\pi\rho}{6}}v\left(\sqrt{2}T-v\right)\right) \\
&\quad + \sqrt{6}e^{-\frac{1}{6}\pi\rho v^2\left(v-\sqrt{2}T\right)^2}\left(\pi\rho v^2\left(2T^2-5\sqrt{2}Tv+7v^2\right)+6\right) \\
&\quad -3\sqrt{6}\left(\pi\rho v^4+2\right)\Bigg]\mathrm{d}v \\
&= \lim_{\rho\to\infty} \int_{\frac{T}{\sqrt{2}}}^{\sqrt{2}T} \frac{4b}{\pi\rho^{3/2}v^3}\Bigg[-\pi\sqrt{\rho}v^2\big(\pi\rho v\big(-2\sqrt{2}T^3+12T^2v \\
&\quad -12\sqrt{2}Tv^2+7v^3\big)\big)\Bigg]\mathrm{d}v \\
&= \frac{7}{4}b\pi T^4
\end{aligned}
\tag{4.53}
$$

such that the overall contribution of the second term is $\mathrm{LHS}_2 = \mathrm{LHS}_{2,\mathrm{I}} + \mathrm{LHS}_{2,\mathrm{II}} = 2b\pi T^4$, combining with LHS_1 to give $2b\pi T^4 + 4\pi T^2$, which matches with the RHS. If the conjecture holds for this case, these two terms give sufficient contributions and the function $\omega(u, v, \rho, T)$ should provide no contribution. While this is encouraging, further work must be done to show that the remaining terms vanish when integrated over the region and the limit is taken if we are to consider this as actual evidence in favour of the conjecture.

Chapter 5

Discussion

We find that the Benincasa-Dowker conjecture is well motivated and evidence in favour of it continues to pile up for numerous spacetimes, including for the new examples we explored in this work.

While there has not yet been a counter-example that has disproved the conjecture, a proof of the conjecture would be desirable and an important step towards an intermediate causal set dynamics in the sum-over-histories framework.

In terms of further evidence for the conjecture, the development by Machet and Wang giving evidence for the conjecture in the form of a causal interval in a Riemann normal neighbourhood of arbitrary curvature [30] is welcome and could form a basis for further work on examples with arbitrary curvature away from the low curvature regime. So far all the examples discussed, including our original results, have come with caveats, applying only where curvature remains low. If the conjecture could be shown to hold for any general causal interval spacetime, without caveats, that would be a significant indication that the conjecture is true.

Dowker suggested that this could be done computationally via simulated sprinkled causets [28], which could complement any analytical developments for that example. The issue remains that this is difficult to show analytically, although it should be more achievable in the short term than a full proof of the conjecture.

A key issue that has been noted by Dowker, Machet and Wang is the nature of the boundary contribution: from where does it arise? It is difficult to see from the calculations that the contribution comes exclusively from the joint. Computational results for the causet

d'Alembertian of a constant field evaluated at elements near the joint could be a next step for this specific problem, giving further grounding for the argument for the conjecture given by Dowker in [28].

Further work could also be done by studying the behaviour of the BDG action on more general manifold shapes, such as those that are not globally hyperbolic and thus can have timelike boundaries, the vicinity of which is a region where the contribution to the BDG action remains untested. For these spacetimes we would expect the conjecture to not hold, as the argument for the conjecture given by Dowker would not be consistent with the timelike boundary. For example, consider a flat 2D rectangle spacetime, bounded by two timelike sides and two spacelike sides. The joint would consist of the two timelike sides, as both future and past directed causal curves could leave the spacetime through those boundaries. However, this is not covered by the argument given by Dowker as the idea of the causet elements in the joint 'not having enough room' in their future or their past does not apply; the elements in the immediate vicinity of the timelike boundaries are not bounded in such a way. Therefore it is expected that the conjecture would not hold and this is why the conjecture is restricted to globally hyperbolic spacetimes. However, the behaviour of the causet d'Alembertian of a constant field near these boundaries is still an interesting avenue to explore.

Chapter 6

Summary

In Chapter 1, we explored the issues that crop up when trying to formulate a quantum theory of gravity. We discussed how our two dominant theories for the large scale and the small scale, GR and QFT respectively, are fundamentally incompatible with another, demanding a new approach to the problem. We also investigated the problems we encounter with the continuum, such as the infinities that pop up in QFT which mean that a quantum field theory of gravity is non-renormalisable, and the singularities in GR.

In Chapter 2, we introduced the causal sets programme by first discussing the motivation for viewing spacetime as a discrete manifold. We defined a causal set as a locally finite partially ordered set, and discussed the work done on causal structure that allowed causal sets to become a viable approach to quantum gravity. Hasse diagrams were introduced to help us visualise causal sets, and ideas behind the connection between the underlying causal set and the emergent continuum were discussed. We introduced Poisson sprinkling as a Lorentz invariant way to define a faithful embedding for a causal set, and gave two examples of dimension estimators: the Myrheim-Meyer dimension and the midpoint-scaling dimension. We also discussed the sample space of all causal sets and how rare manifold-like causal sets were in comparison to layered causets such as the Kleitman-Rothschild causets.

Classical Sequential Growth and transitive percolation were introduced as classical stepping stones towards a quantum dynamics of causal sets, and the basis of Quantum Sequential Growth as quantum measure theory was summarised. There was then brief discussion around the use of the sum-over-histories approach as an intermediate quantal dynamics for causal sets.

In Chapter 3, we introduced the causal set d'Alembertian, and reviewed how Benincasa, Dowker and Glaser used the d'Alembertian to construct the scalar curvature of a causal set and then the causal set action. We also discussed how, in the continuum limit of the action, we may expect contributions from the intersection of the past and the future boundary of a manifold (referred to as the joint) that are separate to the expected bulk Einstein-Hilbert term.

In Chapter 4, we stated the Benincasa-Dowker conjecture, a conjecture which claims that, in the continuum limit, the mean of the random discrete action (i.e. the BDG action calculated on a causal set $\mathcal{C}$ generated by sprinkling a globally hyperbolic Lorentzian manifold $\mathcal{M}$) gives the Einstein-Hilbert action calculated on $\mathcal{M}$ plus the volume of the joint. We discussed the existing evidence for this conjecture in the literature, and proceeded to some original results which gave further evidence. We gave evidence for four cases: the 2D flat and curved (conformally flat) null trapezium, the 2D flat overlapping causal diamonds, and the 4D flat null cone. Encouraging work on a fifth case (4D curved null cone) was also presented, which is yet to be completed.

In Chapter 5, we discussed the BD conjecture and the new evidence we presented, as well as the difficulty in achieving analytical results for further evidence from more general spacetimes. It was suggested that computational results from simulated sprinkled causal sets could play an important role in complementing any further analytical developments, such as with elements near the joint to give a stronger basis for the argument for the conjecture as given by Dowker. We also suggested further work on evaluating the BDG action for non-globally-hyperbolic spacetimes, particularly the contribution that comes from the immediate vicinity of timelike boundaries.

Acknowledgements

Firstly, I would like to thank my supervisor, Fay Dowker, for being an inspirational physicist and a caring supervisor. I have found this to be a tough year due to personal circumstances, and have had bad, unproductive weeks between the good, productive ones. But throughout the project Fay allowed me to work at my own pace, always being supportive if I needed a break or if something hadn't quite worked out as intended. I really feel that it is in large part thanks to her guidance and wisdom that I've been able to produce this dissertation, with novel results, which I am incredibly proud of.

Thank you to my mum, my dad, and my brother for being there for me as always and without whom I would've struggled to make it through a global pandemic.

And finally, thanks to Imperial, the university I'm saying goodbye to after five long years. I've learnt a lot here, about both physics and life, and I'm fortunate enough to have got to know fantastic people and made great lifelong friends. There have been good times, there have been bad, but either way, these have been the most formative years of my life and I will cherish them always.

Bibliography

[1] CERN, "LHC Season 2: facts and figures," Jul 2018.

[2] T. Rothman and S. Boughn, "Can gravitons be detected?," *Foundations of Physics*, vol. 36, no. 12, pp. 1801–1825, 2006.

[3] L. Bombelli, J. Lee, D. Meyer, and R. D. Sorkin, "Space-time as a causal set," *Phys. Rev. Lett.*, vol. 59, pp. 521–524, Aug 1987.

[4] J. Myrheim, "Statistical geometry," tech. rep., 1978.

[5] S. W. Hawking, A. R. King, and P. J. McCarthy, "A new topology for curved space–time which incorporates the causal, differential, and conformal structures," *Journal of Mathematical Physics*, vol. 17, no. 2, pp. 174–181, 1976.

[6] D. B. Malament, "The class of continuous timelike curves determines the topology of spacetime," *Journal of Mathematical Physics*, vol. 18, no. 7, pp. 1399–1404, 1977.

[7] B. Riemann, "On the hypotheses which lie at the bases of geometry," *Nature*, vol. 8, pp. 36–37, 1873.

[8] M. Beller, R. S. Cohen, and R. Jurgen, *Einstein in context*. Cambridge University Press, 1993.

[9] S. Surya, "The causal set approach to quantum gravity," *Living Rev. Rel.*, vol. 22, no. 1, p. 5, 2019.

[10] D. M. T. Benincasa and F. Dowker, "Scalar curvature of a causal set," *Phys. Rev. Lett.*, vol. 104, p. 181301, May 2010.

[11] E. C. Zeeman, "Causality implies the Lorentz group," *Journal of Mathematical Physics*, vol. 5, no. 4, pp. 490–493, 1964.

[12] A. Levichev, "Prescribing the conformal geometry of a Lorentz manifold by means of its causal structure," in *Soviet Math. Dokl*, vol. 35, p. 133, 1987.

[13] F. Dowker, "Introduction to causal sets and their phenomenology," *General Relativity and Gravitation*, vol. 45, no. 9, pp. 1651–1667, 2013.

[14] D. A. Meyer, *The dimension of causal sets.* PhD thesis, Massachusetts Institute of Technology, 1988.

[15] R. D. Sorkin, "Causal sets: Discrete gravity (notes for the Valdivia summer school)," *Proceedings of the Valdivia Summer School, Valdivia, Chile*, 2002.

[16] D. D. Reid, "Manifold dimension of a causal set: Tests in conformally flat spacetimes," *Phys. Rev. D*, vol. 67, p. 024034, Jan 2003.

[17] D. J. Kleitman and B. L. Rothschild, "Asymptotic enumeration of partial orders on a finite set," *Transactions of the American Mathematical Society*, vol. 205, pp. 205–220, 1975.

[18] D. P. Rideout and R. D. Sorkin, "Classical sequential growth dynamics for causal sets," *Phys. Rev. D*, vol. 61, p. 024002, Dec 1999.

[19] R. D. Sorkin, "Quantum mechanics as quantum measure theory," *Modern Physics Letters A*, vol. 09, no. 33, pp. 3119–3127, 1994.

[20] R. D. Sorkin, "Quantum measure theory and its interpretation," in *3rd Workshop on Physics and Experiments with e+ e- Linear Colliders (LCWS 95)*, 7 1995.

[21] D. M. T. Benincasa, *The action of a causal set.* PhD thesis, Imperial College London, 2013.

[22] R. D. Sorkin, "Does locality fail at intermediate length-scales?," in *Approaches to Quantum Gravity: Toward a New Understanding of Space, Time and Matter* (D. Oriti, ed.), ch. 3, pp. 26–43, Cambridge University Press, 2009.

[23] J. Henson, "The causal set approach to quantum gravity," in *Approaches to Quantum Gravity: Toward a New Understanding of Space, Time and Matter* (D. Oriti, ed.), ch. 3, pp. 393–413, Cambridge University Press, 2009.

[24] F. Dowker and L. Glaser, "Causal set d'Alembertians for various dimensions," *Classical and Quantum Gravity*, vol. 30, p. 195016, Sep 2013.

[25] L. Glaser, "A closed form expression for the causal set d'Alembertian," *Classical and Quantum Gravity*, vol. 31, p. 095007, Apr 2014.

[26] S. P. Loomis and S. Carlip, "Suppression of non-manifold-like sets in the causal set path integral," *Classical and Quantum Gravity*, vol. 35, p. 024002, dec 2017.

[27] D. M. T. Benincasa, F. Dowker, and B. Schmitzer, "The random discrete action for two-dimensional spacetime," *Classical and Quantum Gravity*, vol. 28, p. 105018, Apr 2011.

[28] F. Dowker, "Boundary contributions in the causal set action," *Classical and Quantum Gravity*, vol. 38, p. 075018, Mar 2021.

[29] M. Buck, F. Dowker, I. Jubb, and S. Surya, "Boundary terms for causal sets," *Classical and Quantum Gravity*, vol. 32, p. 205004, Sep 2015.

[30] L. Machet and J. Wang, "On the continuum limit of Benincasa–Dowker–Glaser causal set action," *Classical and Quantum Gravity*, vol. 38, p. 015010, Dec 2020.

[31] L. Machet and J. Wang, "On the horizon entropy of a causal set," *Classical and Quantum Gravity*, vol. 38, p. 085004, Mar 2021.

Appendix A

GR Preliminaries

In this appendix, we feature some of the preliminaries from GR used in this dissertation.

A.1 Einstein-Hilbert action

The Einstein-Hilbert action is

$$S_{\mathrm{EH}}(\mathcal{M}) = \frac{1}{2\kappa}\int_{\mathcal{M}} \mathrm{d}^d x\sqrt{-g}R \tag{A.1}$$

which is the action for a vaccuum on the manifold. By adding a matter action to the EH action, we find that the resulting equations of motion will be the EFE.

A.2 Alexandrov intervals

We also define $J^+(p)$ as the part of the manifold that lies in the causal future of a point p, and likewise $J^-(p)$ as the causal past of p. The Alexandrov interval meanwhile is the union of the causal future and causal past of two points, i.e. $A(p,q) = J^+(p) \cup J^-(q)$ for $q \in J^+(p)$, forming what is colloquially called a causal diamond.

Appendix B

Coefficients of the BDG action

While given in [25], the closed form expressions for the coefficients in the causal set action are repeated here for convenience.

B.1 Closed form expressions

For even d,

$$\alpha_d = \frac{-(S_{d-2})^{\frac{2}{d}}}{2^{(-\frac{2}{d})}(d(d-1))^{\frac{2}{d}}\Gamma(\frac{2}{d}+1)} \tag{B.1}$$

$$\beta_d = \frac{(S_{d-2})^{\frac{2}{d}}\Gamma(\frac{d}{2}+2)\Gamma(\frac{d}{2}+1)}{2^{-\frac{2}{d}}(d(d-1))^{\frac{2}{d}}\Gamma(\frac{2}{d})\Gamma(d)} \tag{B.2}$$

$$C_i^{(d)} = \sum_{k=0}^{i-1}(-1)^k \frac{(i-1)!\,\Gamma\left(\frac{d}{2}(k+1)+2\right)}{k!(i-1-k)!\,\Gamma(\frac{d}{2}+2)\Gamma(\frac{kd}{2}+1)} \tag{B.3}$$

and for odd d,

$$\alpha_d = \frac{-(S_{d-2})^{\frac{2}{d}}}{2^{(1-\frac{2}{d})}(d(d-1))^{\frac{2}{d}}\Gamma(\frac{2}{d}+1)} \tag{B.4}$$

$$\beta_d = \frac{(S_{d-2})^{\frac{2}{d}}(d+1)}{2^{(d-\frac{2}{d})}(d(d-1))^{\frac{2}{d}}\Gamma(\frac{2}{d}+1)} \tag{B.5}$$

$$C_i^{(d)} = \sum_{k=0}^{i-1}(-1)^k \frac{(i-1)!\,\Gamma\left(\frac{d}{2}(k+1)+\frac{3}{2}\right)}{k!(i-1-k)!\,\Gamma(\frac{d+3}{2})\Gamma(\frac{kd}{2}+1)} \tag{B.6}$$

where S_{d-2} is the volume of the $(d-2)$-sphere.

B.2 Calculated coefficients for 2D and 4D

In [13], the coefficients were calculated explicitly for $d = 1$ through to $d = 7$.

In 2D,

$$\alpha_2 = -2 \qquad \beta_2 = 4 \qquad C_i^{(2)} = (1, -2, 1) \tag{B.7}$$

In 4D,

$$\alpha_4 = -\frac{2}{\Gamma(\frac{3}{2})}\sqrt{\frac{\pi}{6}} \qquad \beta_4 = -\alpha_4 \qquad C_i^{(4)} = (1, -9, 16, -8) \tag{B.8}$$